CHAPTER 6

Surface Waves

6.1 Travelling versus standing waves . Summing up fundamental mode spheroidal modes results in a seismogram consisting of fundamental mode Rayleigh waves. Similarly, summing up fundamental toroidal modes results in a seismogram consisting of fundamental mode Love waves. In some cases, it is better to think of the seismogram as a sum of modes but, because the fundamental mode surface wave packets often arrive at a seismometer separated from the overtone wave packets, a travelling wave representation is often better for data analysis. The formal relationship between standing modes and travelling waves is discussed in detail by Gilbert (1976) but we do not need such a formal analysis here. We begin by considering propagation on a spherical Earth and, for simplicity, we consider the expression for the excitation of a single mode by an explosive source recorded on a vertical component receiver. Combining 5.42 with 5.57 gives:

$$s(t) = \mathrm{Re}[UE \sum_m Y_l^{m*}(\theta_s, \phi_s) Y_l^m(\theta_r, \phi_r) e^{i\bar{\omega}t}\,].$$

Using the addition rule for spherical harmonics we get

$$s(t) = \mathrm{Re}[UE \sqrt{\frac{2l+1}{4\pi}}\, Y_l^0(\Delta) e^{i\bar{\omega}t}\,]$$

where Δ is epicentral distance. For large l, we can use the asymptotic form (B.23) of Y_l^m

$$Y_l^0(\Delta) = \frac{1}{\pi\sqrt{\sin\Delta}} \cos\,[(l+\tfrac{1}{2})\Delta - \frac{\pi}{4}].$$

This looks like a plane wave $A\cos kx$ with x being distance, $x = a\Delta$ (a is the radius of the Earth) and k is wavenumber which is related to harmonic degree by Jeans' formula:

$$ka = l + \tfrac{1}{2}$$

Thus, we can write

$$s(t) \propto e^{i(\omega t - kx)}$$

($-kx$ since we want a wave propagating in positive direction with increasing time). Surface wave propagation is dispersive, i.e., different frequency components of a surface wave packet travel at different speeds ($k = k(\omega)$) so that the wave packet spreads out over time. This dispersion is usually measured by the phase velocity: $c(\omega) = \omega/k$ which measures the speed at which a peak or a trough travels.

Since mode summation is essentially integration over frequency, a surface wave seismogram can be written as

$$s(x,t) = \int A(\omega) e^{i(\omega t - k(\omega)x)}\, d\omega \tag{6.1}$$

where $A(\omega)$ represents the effects of the source and is slowly varying as a function of frequency. (There are also some phase shifts associated with passage through the pole but we ignore those for now). Most of the contributions to this integral will come from places where the phase $f = \omega t - k(\omega)x$ is stationary (i.e. $df/d\omega = 0$) – otherwise the integrand is rapidly oscillating and will end up cancelling out in the integral. If ω_s is the point where the phase is stationary occurs, we have

$$t - \frac{dk}{d\omega}(\omega_s)x = 0$$

Define a new velocity, U, such that

$$U = \frac{x}{t} = \frac{d\omega}{dk}$$

Then we see that a particular value of frequency and wavenumber found at x_1, t_1 will be found at x_2, t_2 provided that $x_1/t_1 = x_2/t_2$, i.e. it has travelled with velocity U. Thus the energy associated with a particular frequency group centered on ω_s travels with the "group velocity", $U(\omega_s)$. From $c = w/k$, we find that

$$\frac{c}{U} = 1 - \frac{\omega}{c}\frac{dc}{d\omega}$$

so $c = U$ only when c is independent of frequency and we have an undispersed signal. Phase and group velocity for fundamental Love and Rayleigh waves for model PREM are shown in figure 1.

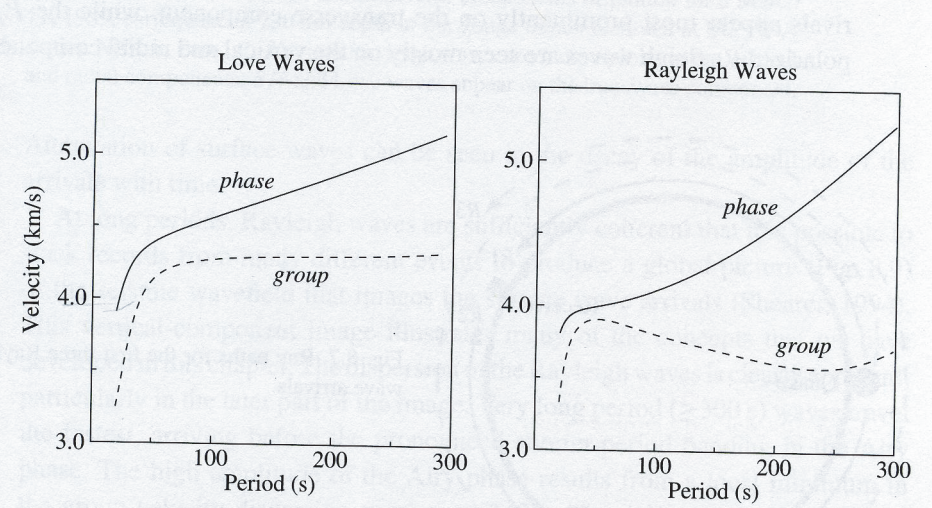

Fig. 8.6. Fundamental Love and Rayleigh dispersion curves computed from the isotropic PREM model (courtesy of Gabi Laske).

The difference between phase and group velocity can be very clearly seen in the stack of long period records shown in figure 2.

On an aspherical Earth, it is natural to think of plane wave surface propagation with the dispersion term now the average dispersion along the great circle arc between source and receiver, i.e.

$$e^{ikx} \Longrightarrow e^{i\bar{k}x} \qquad \text{where} \qquad \bar{k} = \frac{1}{x}\int_0^x k(x')dx'.$$

We shall prove later that the surface wave phase $\bar{k}x$ is insensitive to small departures from great circle wave propagation – a consequence of Fermat's principle. Surface wave analysis is conducted at fixed period so we think of wave number as

$$k = k(\omega, \theta, \phi)$$

or in terms of phase velocity:

$$c(\omega, \theta, \phi) = c_0(\omega) + \delta c(\omega, \theta, \phi)$$

where $c_0(\omega)$ is the mean phase velocity at frequency ω. The primary type of data used to constrain the phase velocity is the measurement of phase, though it is also possible to use surface wave amplitudes and arrival angles to help constrain phase velocity (see later).

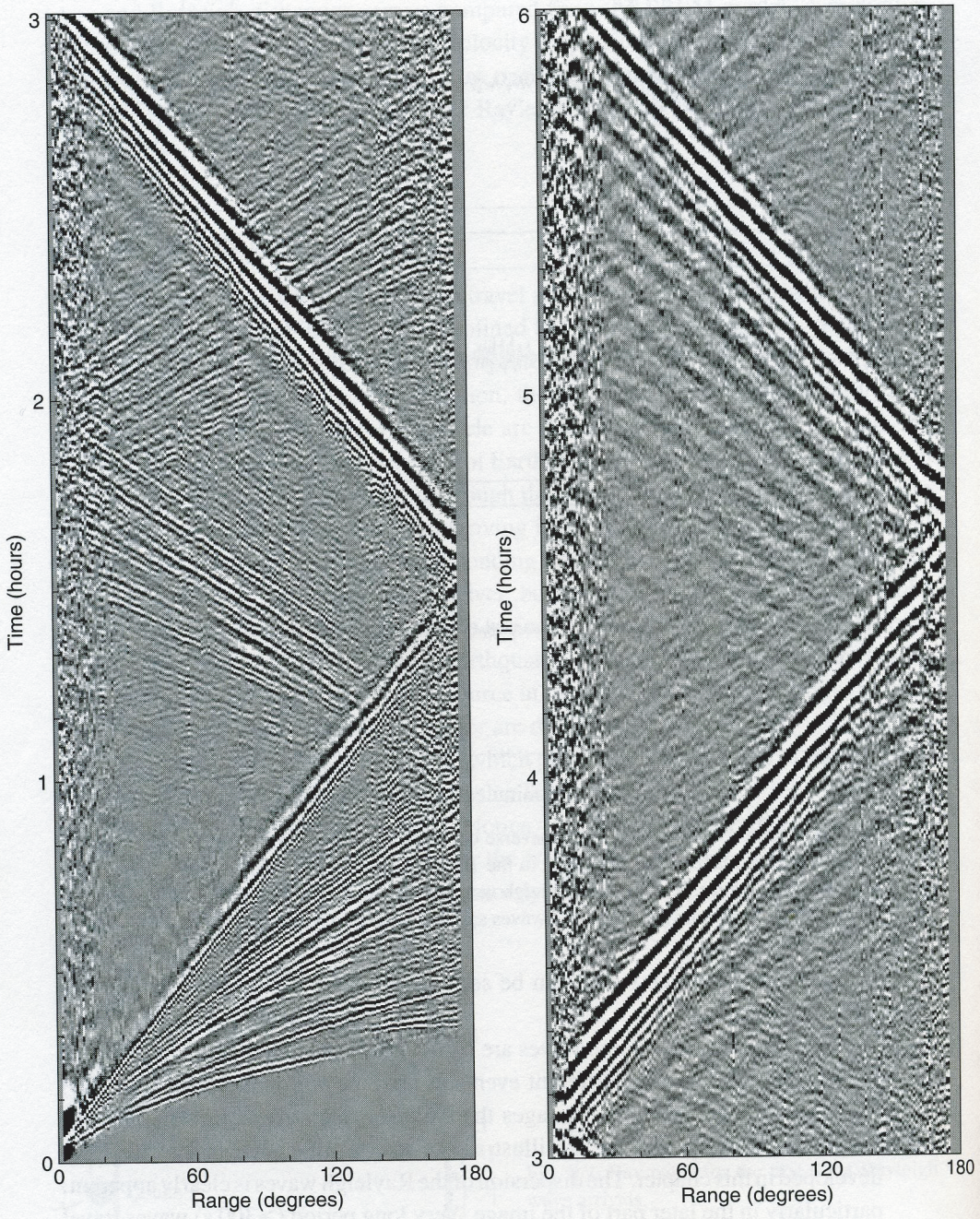

Fig. 8.9. An image of Earth's long-period seismic response on vertical component seismographs as a function of time and distance to an earthquake. Positive amplitudes are shown as black, and negative amplitudes are shown as white. The Rayleigh wave arrivals $R1$ and $R2$ are visible in the left panel showing the first 3 hours of data, whereas $R3$ and $R4$ are seen on the right panel.

6.2 Measuring phase . It might be thought that measuring phase simply means Fourier transforming a seismogram (e.g. equation 6.1) and looking at the resulting phase of the fourier transform. Of course, phase is a very strong function of frequency and wraps through cycles of 2π very rapidly. Unwrapping phase is

difficult and, in any case, phase estimated by this technique will be biased because of the implicit frequency averaging involved in Fourier transforming. It is therefore best to measure relative phase between two very similar signals. These might be the data and a synthetic or it might be an R3 orbit compared with an R1 orbit which has been filtered to take account of the great circle dispersion and attenuation (this latter measurement has the benefit of not needing to know the properties of the source). It is very important that the two signals are well-aligned in time before the measurement is made.

One dispersion measurement technique is based on a cross-spectral method [Berger et al., 1979] of estimating a transfer function. Let $F_s(\omega), F_o(\omega)$ be the spectra of the synthetic and observed time series which are related to each other by the linear operator $T(\omega)$ which is the transfer function. The cross-spectral estimate of $T(\omega)$ is

$$T(\omega) = \frac{F_s^*(\omega)F_o(\omega)}{F_s^*(\omega)F_s(\omega)} = \frac{C_{12}(\omega)}{C_{11}(\omega)}.$$

where $C_{11}(\omega)$ is the power spectrum of the synthetic and $C_{12}(\omega)$ is the cross-spectrum between the observed and synthetic signals. Experiments with simple synthetic signals have shown that a set of prolate spheroidal wave function eigentapers [Slepian, 1978] applied in a multi-taper technique [Thomson, 1982] induces less bias in the phase measurements than any other window (except for the boxcar window) if the two signals are not perfectly aligned. This is especially true for small amplitude signals. Apart from the fact that poor resistance to bias in the presence of noise rules out the boxcar window, the multi-taper technique also has the benefit of providing error estimates. The first five of the 2.5π–prolate tapers give 5 independent spectral estimates in the frequency range of interest: 3–15 mHz (the average taper length being 35 min). The five tapers are orthogonal and the phase can be determined in a least squares procedure where

$$\|\mathbf{F}_o(\omega) - T \cdot \mathbf{F}_s(\omega)\|^2$$

is to be minimized. $\mathbf{F}_o$ and $\mathbf{F}_s$ are vectors whose components are the spectral estimates at fixed frequency using one of the prolate tapers. The least-squares estimate of the transfer function then is

$$T(\omega) = \frac{\mathbf{F}_o(\omega) \cdot \mathbf{F}_s^*(\omega)}{\mathbf{F}_s(\omega) \cdot \mathbf{F}_s^*(\omega)}. \tag{6.2}$$

The errors in the transfer function are obtained using a jackknife procedure.

If the synthetic is substantially different from the observed signal, the transfer function should be obtained by iterating the above procedure though this is not necessary when studying long-period surface waves.

Once the transfer function is determined for a pair of observed and synthetic data, the complex transfer function at frequency ω is related to phase and attenuation structure for one mode (the fundamental mode in our case) by

$$T(\omega) = e^{-\delta\bar{\gamma}(\omega)x} e^{-i\delta\bar{k}(\omega)x} \tag{6.3}$$

where x is the travel path along the great circle arc between source and receiver and $\delta\bar{\gamma}$ and $\delta\bar{k}$ are the mean measured anomalies of damping parameter, γ, and wave number, k, or phase velocity $c(\omega) = \omega/k$ with respect to the model along the great circle. The parameter γ is a measure of anelastic attenuation only in the absence of focusing–defocusing effects which is not true for a laterally heterogeneous Earth.

6.3 Inverting phase for phase velocity maps . The measured perturbation in phase can be written

$$\delta\Psi = \delta\bar{k}a\Delta = -\frac{\omega a}{c_0} \int_0^\Delta \frac{\delta c(\theta,\phi)}{c_0}\, d\gamma \tag{6.4}$$

where the integral is taken over the great circle path from source to receiver. This equation can be converted into a linear inverse problem for the perturubation in phase velocity if we parameterize the lateral variations in phase velocity in some way. Parameterizations in terms of both local bases (e.g. pixels) and global bases

(e.g. spherical harmonics) have both been done. The latter is more computationally intensive since the resulting matrices are full (see below) but results in a model which is readily differentiable for use in ray tracing and the like. We therefore consider this case first. At a fixed frequency, the geographic dependence of $\delta c/c_0$ is expanded in spherical harmonics:

$$\frac{\delta c(,\theta,\phi)}{c_0} = \sum_{s,t} a_s^t(\omega) Y_s^t(\theta,\phi)$$

and

$$\delta\Psi = -\frac{\omega a}{c_0} \sum_{s,t} a_s^t \int_0^\Delta Y_s^t(\theta,\phi)\, d\gamma \tag{6.5}$$

Suppose we look at great circle dispersion then (using 5.64)

$$\frac{1}{2\pi} \int_{\Theta,\Phi} Y_s^t(\theta,\phi)\, d\lambda = P_s(0) Y_s^t(\Theta,\Phi)$$

$$\delta\Psi = -\frac{\omega a}{c_0} \sum_{s,t} a_s^t P_s(0) Y_s^t(\Theta,\Phi) \tag{6.6}$$

where (Θ,Φ) is the pole of the great circle joining source and receiver. Note that all sensitivity to odd-order structure is lost ($P_s(0) = 0$ if s is odd) so we must look at minor and major arc integrals if we are to recover odd order structure. Equation 6.5 can be put in terms of a linear inverse problem by writing out the a_s^t as a linear vector indexed by j. Then the i'th datum ($y_i = \delta\Psi_i$) is related to a_j by

$$G_{ij} = -\frac{\omega a}{c_0} P_j(0) Y_j(\Theta_i,\Phi_i)$$

giving

$$\mathbf{y} = \mathbf{G}\cdot\mathbf{a} \tag{6.7}$$

To do minor and major arcs, the integral over arc-distance is most easily done by rotating the coordinate system such that the great circle is on the equator. Such a coordinate transform for spherical harmonics can be written

$$Y_s^t(\theta',\phi') = \sum_{m=-s}^{s} B_{mt} Y_s^m(\theta,\phi).$$

Note that a spherical surface harmonic of degree s in the new coordinate system is a linear combination of the $2s+1$ harmonics of degree s in the old coordinate system. Thus

$$\frac{\delta c(\theta',\phi')}{c_0} = \sum_{s,t} a_s^t Y_s^t(\theta',\phi') = \sum_{s,t} a_s^t \sum_{m=-s}^{s} B_{mt} Y_s^m(\theta,\phi).$$

Identify

$$b_s^m = \sum_t a_s^t B_{mt}$$

so that

$$\frac{\delta c(\theta',\phi')}{c_0} = \sum_{s,m} b_s^m Y_s^m(\theta,\phi).$$

In the transformed system with the path along the equator, $Y_s^t(\theta,\phi)$ becomes

$$Y_s^m(\frac{\pi}{2},\Delta') = X_s^m(\frac{\pi}{2})e^{im\Delta'},$$

where Δ' is the travel distance along the equator. The integral along the ray path is now just an integral over $\exp(im\Delta')$ from zero to Δ:

$$\begin{aligned}\delta\Psi &= -\frac{\omega a}{c_0}\sum_{s,m} b_s^m X_s^m(\frac{\pi}{2})\frac{1}{im}(e^{im\Delta}-1)\\ &= -\frac{\omega a}{c_0}\sum_{s,m}\sum_t a_s^t B_{mt} X_s^m(\frac{\pi}{2})\frac{1}{im}(e^{im\Delta}-1)\end{aligned} \tag{6.8}$$

This can be put in the form (6.7) for an inverse problem for the a_s^t given many observations of phase perturbation, $\delta\Psi$. Note that the transformation matrix B_{mt} is straightforward to compute (Edmonds, 1960; Backus, 1964) but the calculation is omitted here.

When making phase velocity maps, we will often want to impose constraints on the allowable roughness at the same time as trying to fit the data. When we have a spherical harmonic representation, it is convenient to use the squared horizontal Laplacian (∇_1^2) integrated over the unit sphere as a measure of roughness. Thus we might want to minimise

$$\int_\Omega |\nabla_1^2\delta c(\theta,\phi)|^2 d\Omega = \sum_s^t s^2(s+1)^2|a_s^t|^2$$

We now minimise

$$(\mathbf{G}\cdot\mathbf{a}-\mathbf{y})^T\cdot(\mathbf{G}\cdot\mathbf{a}-\mathbf{y}) + \mu\mathbf{a}^T\cdot\mathbf{D}^T\cdot\mathbf{D}\cdot\mathbf{a}$$

with respect to $\mathbf{a}$ where μ is a parameter which controls the amount of smoothing and $\mathbf{D}$ is a diagonal matrix with elements $s(s+1)$. The result is

$$(\mathbf{G}^T\cdot\mathbf{G}+\mu\mathbf{D}^T\cdot\mathbf{D})\cdot\mathbf{a} = \mathbf{G}^T\cdot\mathbf{y}$$

and the square symmetric matrix on the left hand side can be inverted using any number of techniques to get $\mathbf{a}$. Alternatively, we can write this equation in the form:

$$\begin{bmatrix}\mathbf{G}\\ \sqrt{\mu}\mathbf{D}\end{bmatrix}\cdot\mathbf{a} = \begin{bmatrix}\mathbf{y}\\ \mathbf{0}\end{bmatrix} \tag{6.9}$$

and solve this using an SVD to avoid forming the normal equations. Note that if we replace $\mathbf{D}$ with $\mathbf{I}$, we are penalizing the amplitude of the model:

$$\int_\Omega |\delta c(\theta,\phi)|^2 d\Omega$$

This tends to result in models with severely underestimated amplitudes and is not recommended

6.4 Using a local basis . In equation 6.7, the matrix $\mathbf{G}$ will be full because every great circle path samples every spherical harmonic. If instead, we use a local basis to describe $\delta c(\theta,\phi)/c_0$ such as local splines or even just pixels, then each datum will sample only those pixels along the ray path joining source and receiver. In other words, the matrix $\mathbf{G}$ will be very sparse. There exist a large number of good algorithms for solving large sparse systems – we discuss some of these in chapter 7 – and the use of a local basis allows us to go to very fine parameterizations, even on global scales.

All we need to do is to calculate the arc length within each pixel. Consider the following spherical triangle where the colatitude and longitude of the source is θ_0,ϕ_0 and the colatitude and longitude of the receiver is θ_r,ϕ_r.

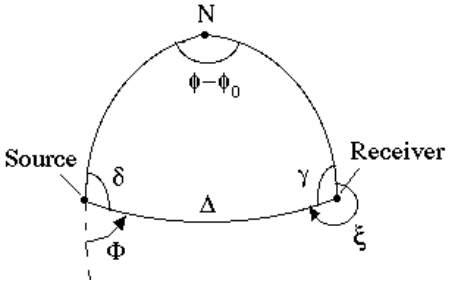

Δ is epicentral distance and δ is the azimuth of the receiver from the source. We compute these first using

$$\cos\Delta = \cos\theta_r \cos\theta_0 + \sin\theta_r \sin\theta_0 \cos(\phi_r - \phi_0) \quad \text{and} \quad \sin\Delta = (1 - \cos^2\Delta)^{\frac{1}{2}}$$
$$\cos\delta = (\cos\theta_r - \cos\theta_0 \cos\Delta)/(\sin\theta_0 \sin\Delta) \quad \text{and} \quad \sin\delta = \sin(\phi_r - \phi_0)\sin\theta_r/\sin\Delta$$

There are two special cases we must consider when computing δ: when $\sin\theta_0 = 0$ and when $\sin\Delta = 0$. By considering the limiting behavior of the equations, we find that if $\theta_0 = 0$, then $\delta = \pi - (\phi_r - \phi_0)$ and if $\theta_0 = \pi$, then $\delta = \phi_r - \phi_0$. If $\Delta = 0$, the source and receiver are at the same place and the great circle is undefined. Similarly, if $\Delta = \pi$, the source and receiver are antipodal and the great circle is undefined.

Once we have δ, we can compute the location of any point (θ, ϕ) on the great circle at distance Δ' from the source using

$$\cos\theta = \cos\Delta' \cos\theta_0 + \sin\Delta' \sin\theta_0 \cos\delta \quad \text{and} \quad \sin\theta = (1 - \cos^2\theta)^{\frac{1}{2}}$$
$$\cos(\phi - \phi_0) = (\cos\Delta' - \cos\theta_0 \cos\theta)/(\sin\theta_0 \sin\theta) \quad \text{and} \quad \sin(\phi - \phi_0) = \sin\Delta' \sin\delta/\sin\theta$$

It is usually fastest to use the ACOS function to compute θ and this produces a result on $0 \le \theta \le \pi$:

$$\theta = \text{ACOS}(\cos\Delta' \cos\theta_0 + \sin\Delta' \sin\theta_0 \cos\delta)$$

Also, since both $\sin\theta$ and $\sin\theta_0$ are positive, it is most efficient to compute $\phi - \phi_0$ using the ATAN2 function as

$$\phi = \phi_0 + \text{ATAN2}(\sin\Delta' \sin\delta \sin\theta_0, \cos\Delta' - \cos\theta_0 \cos\theta)$$

In these equations, both $\sin\delta \sin\theta_0$ and $\sin\theta_0 \cos\delta$ can be pre-computed. Note that the last of these equations will fail if the source is at a geographic pole (both arguments become zero), however, it is obvious that in this situation, the longitude of the great circle is just the longitude of the receiver, ϕ_r or $\phi_r + \pi$, depending upon the distance. Another special case is when $\sin\theta = 0$ which means that the point is either at the north or south pole so the longitude is undefined (and can be set to zero) though it is actually more efficient to ignore this case and let the relations above produce a number. If we let $C_1 = (\cos\theta_r - \cos\theta_0 \cos\Delta)/\sin\Delta$ and $C_2 = \sin\delta \sin\theta_0$, then the following pseudo-code works

$$\begin{aligned}
x &= \cos\Delta' \\
y &= \sin\Delta' \\
z &= x * \cos\theta_0 + y * C_1 \\
\theta &= \text{ACOS}(z) \\
\phi &= \phi_0 + \text{ATAN2}(y * C_2, x - \cos\theta_0 * z)
\end{aligned}$$

An alternative method of moving around the great circles involves the use of Euler angles but this is less efficient. We now step around the great circle in small steps and record which pixel we are in at each step. Summing up all steps for each pixel then gives the arc length for that pixel. Let us call this arc length for the i'th datum and the j'th pixel L_{ij} then the discretized version of 6.4 is just

$$\delta\Psi_i = -\frac{\omega a}{c_0} \sum L_{ij} (\frac{\delta c}{c_0})_j$$

where $(\delta c/c_0)_j$ is the relative perturbation in phase velocity in the j'th pixel.

6.5 Recovering Earth structure . The upshot of all this work are maps of perturbation in phase velocity at a variety of frequencies (see maps on folowing pages). The final step in this clasical analysis is to use these maps to obtain models of structure inside the Earth. We can typically do surface wave phase analysis in the period band 300 to 30 seconds. The longest periods sample into the transition zone of the Earth while the shortest periods are mainly sensitive to crust and upper-lithosphere structure. The computation of sensitivity to structure as a function of depth for a Rayleigh or Love wave at a given frequency is straightforward – in fact we have already computed these sensitivities in chapter 4 for the equivalent fundamental spheroidal and toroidal modes. There, we computed the perturbation in a mode frequency at fixed harmonic degree (wavenumber). Here, we want the perturbation in phase velocity (or wavenumber) at fixed frequency. The relationship between these can be gotten from the following relation:

$$\left(\frac{\partial\omega}{\partial m}\right)_k \left(\frac{\partial k}{\partial\omega}\right)_m \left(\frac{\partial m}{\partial k}\right)_\omega = -1 \qquad \text{(chain rule)} \tag{6.10}$$

where m is a model parameter. Rearranging gives

$$\frac{1}{\omega}\left(\frac{\partial\omega}{\partial m}\right)_k = \frac{U}{c}\cdot\frac{1}{c}\left(\frac{\partial c}{\partial m}\right)_\omega \tag{6.11}$$

This allows us to compute relative perturbations in phase velocity due to a perturbation in a model parameter from the known kernels for the perturbation in frequency (see equation 4.56). Before we consider this inversion in more detail (in the next chapter), we note that group as well as phase velocity can be measured and is actually a more robust measurement at high frequencies so we make a short digression on surface wave group velocity.

6.6 Group velocity . The main problem with a phase analysis occurs at relatively high frequencies where it is possible for wave packets to arrive more than a cycle out of phase with other wave packets at the same distance. It is possible to avoid this cycle-skipping problem by considering the group velocity. Here, we are interested in the arrival time of a packet of energy with a certain dominant frequency. The traditional way of estimating this is to narrow band-pass the data with a Gaussian window in the frequency domain then form the envelope function of the corresponding time series. The arrival time of the peak of the envelope function is interpreted as the group arrival time for this frequency. Since we are dealing with envelope functions, cycle skipping is not a problem. The classical group velocity analysis uses a suite of Gaussian windows centered on different frequencies then plots the amplitude of the envelope function as a function of time and frequency (figure 5). The peak amplitude is identified with the group arrival time as a function of frequency. This kind of analysis is very time consuming and it is desirable to come up with a more efficient measurement technique. Your author has come up with such a technique based on cross-correlation of envelope functions for all records of an event integrated with a clustering technique to cluster similar envelope functions. This technique results in large datasets of relative group arrival times for a variety of frequencies which, with a few more assumptions, can be converted into absolute group arrival times. At the moment, the technique allows the compilation of 250,000 or more group arrival times for frequencies from 7.5mHz to 25mHz with up to 100,000 times up to frequencies of 35mHz.

The classical theory for interpreting group arrival times closely follows that given for phase above where we assume great circle propagation. Thus, a group arrival time can be written

$$t_g = a \int_0^\Delta \frac{1}{U} d\gamma$$

where the integral is over the great circle path from source to receiver. Taking perturbations around a reference 1D group velocity, U_0, gives

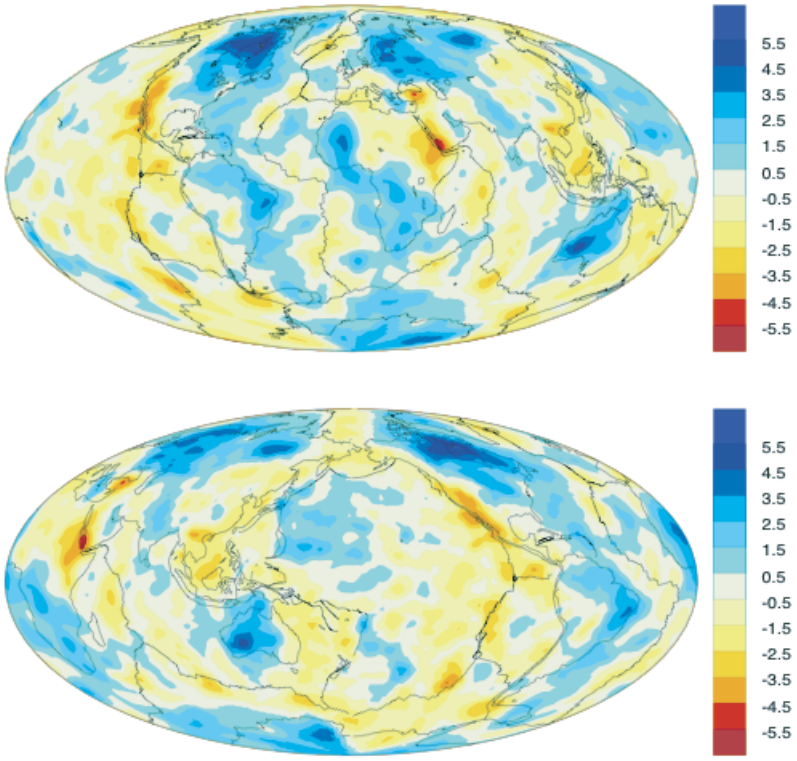

Figure 3 Phase velocity map for Rayleigh waves at 100 seconds

$$\delta t_g = -\frac{a}{U_0}\int_0^{\Delta}\frac{\delta U(\theta,\phi)}{U_0}\,d\gamma \tag{6.12}$$

which is basically the same equation as 6.4 so all the same theory for making phase velocity maps can be applied to making group velocity maps. Group velocity maps for Rayleigh waves at 50 and 100 seconds are shown in figures 5 and 6. Note the much larger amplitudes than found for the equivalent phase velocity maps. This is because the sensitivity kernels for group velocity are more closely concentrated towards the surface and so the measurements are much more sensitive to crustal variations. We can calculate the depth sensitivity kernels numerically from the kernels for phase velocity using the identity

$$\frac{\delta U}{U} = \frac{\delta c}{c} + \frac{\omega U}{c}\frac{\partial}{\partial\omega}(\frac{\delta c}{c})$$

where the last term can be evaluated by differencing phase kernels for modes with adjacent angular orders. Sensitivity kernels for shear velocity are shown in fig 7 where the enhanced sensitvity of group velocity to near surface structure can be seen as well as the larger amplitudes of the kernels which means we will get much bigger signals in group velocity maps. This is clearly demonstrated by comparing Figs 3,4 with figs 5,6.

No inversion is complete without an assessment of resolution and error and we consider these in detail in chapter 7 when we come to do joint inversions for structure using body waves, surface waves and modes. Most methods for computing resolution and error require that the full inverse of the matrix in 6.9 can be computed and this is not usually possible. A good way of estimating errors is to add random noise to the data with the same characteristics (standard deviation) as the noise in the data (or in the residuals after inversion) and then inverting for structure. Several tens of noise sets are used and several tens of models inverted for.

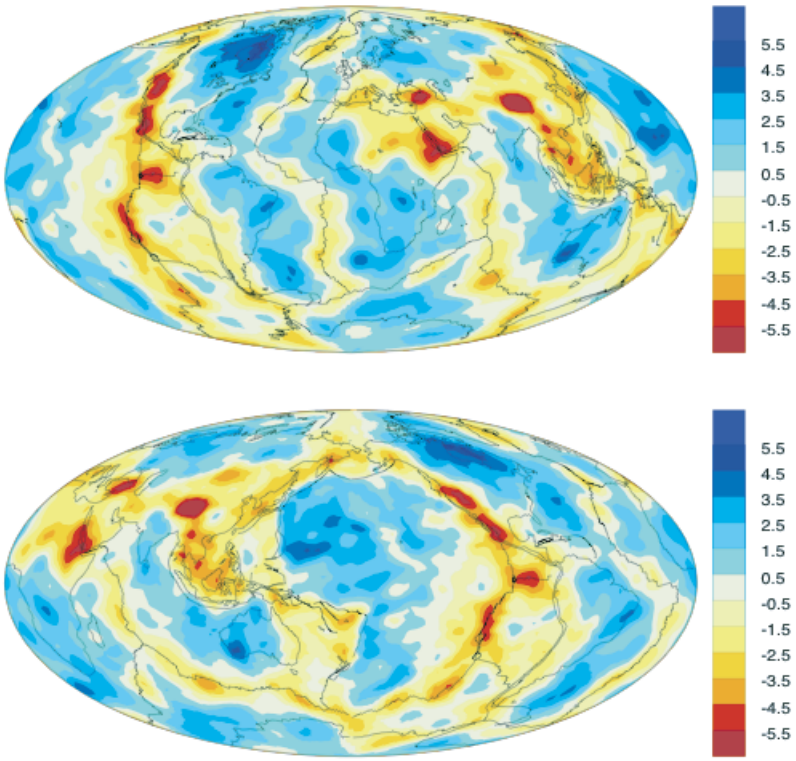

Figure 4 Phase velocity map for Rayleigh waves at 50 seconds

The standard deviation of the mean if the resulting models is a good estimate of the true error. Resolution can be assessed by using spike tests or checkerboard patterns (see chapter 7).

6.7 Computation of group velocity . Since $U = d\omega/dk$ and $ka = l + \frac{1}{2}$, we find that

$$U = a\frac{d\omega}{dl}$$

and we can find group velocity using perturbation theory. Equation 4.55 becomes:

$$\delta\omega_k^2 \int_V \rho_0 \mathbf{s}_k^\star \cdot \mathbf{s}_k \, dV = \int_V \mathbf{s}_k^\star \delta\mathbf{L}(\mathbf{s}_k) \, dV$$

where $\delta\mathbf{L}$ is the result of perturbing $\mathbf{L}$ with respect to l. For example, for toroidal modes, the result is

$$\delta\omega_k^2 \int_0^a \rho_0 N r^2 \, dr = \int_0^a (2l+1)\mu W^2 \, dr$$

This standard method of computing group velocity using perturbation theory does not give quite the right answer when the model includes physical dispersion because this latter effect contributes to the frequency dependence of the phase velocity. If we use the standard form for physical dispersion where Q_s is independent of frequency then

$$c(\omega) = c_0 \left[1 + \frac{1}{\pi Q_s} log\left(\frac{\omega}{\omega_0}\right)\right]$$

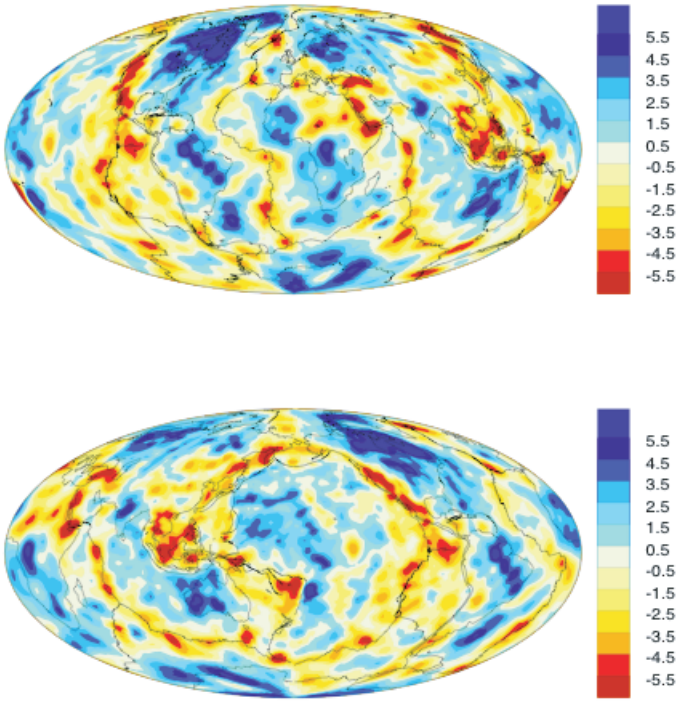

Figure 5 Group velocity map for Rayleigh waves at 100 seconds

where c_0 is the phase velocity at the reference frequency or in the limit of no attenuation. Note that Q_s is "spatial" Q which appears in the definition of the complex wavenumber. It is related to "temporal" Q, Q_t, by

$$\frac{1}{Q_t} = \frac{U}{c}\frac{1}{Q_s}$$

We approach the computation of the correction to the group velocity using the exact relationship:

$$\frac{\delta U}{U} = \frac{\delta c}{c} + \frac{\omega U}{c}\frac{\partial}{\partial \omega}\left(\frac{\delta c}{c}\right)$$

where, in this case, $\delta c/c$ is the relative perturbation in phase velocity due to physical dispersion. For our simple dispersion rule

$$\frac{\delta c}{c} = \frac{1}{\pi Q_s} log\left(\frac{\omega}{\omega_0}\right)$$

so

$$\frac{\delta U}{U} = \frac{\delta c}{c} + \frac{\omega U}{c}\frac{1}{\pi Q_s \omega} = \frac{\delta c}{c} + \frac{1}{\pi Q_s}\frac{U}{c} = \frac{\delta c}{c} + \frac{1}{\pi Q_t}$$

This makes it easy to see how you would compute the perturbation to the group velocity for any dispersion rule. For example, another dispersion rule due to Doornbos is:

$$\frac{\delta c}{c} = -\frac{1}{2\pi Q_s} log\left(1 + \frac{1}{\omega^2 \tau^2}\right)$$

which reduces to the simple case when $\omega\tau$ is much less than one. This dispersion rule gives

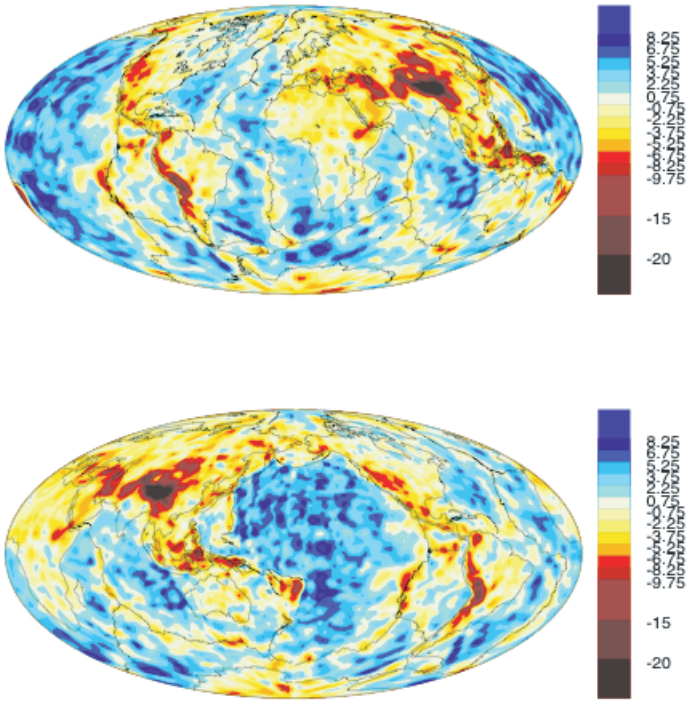

Figure 6 Group velocity map for Rayleigh waves at 50 seconds

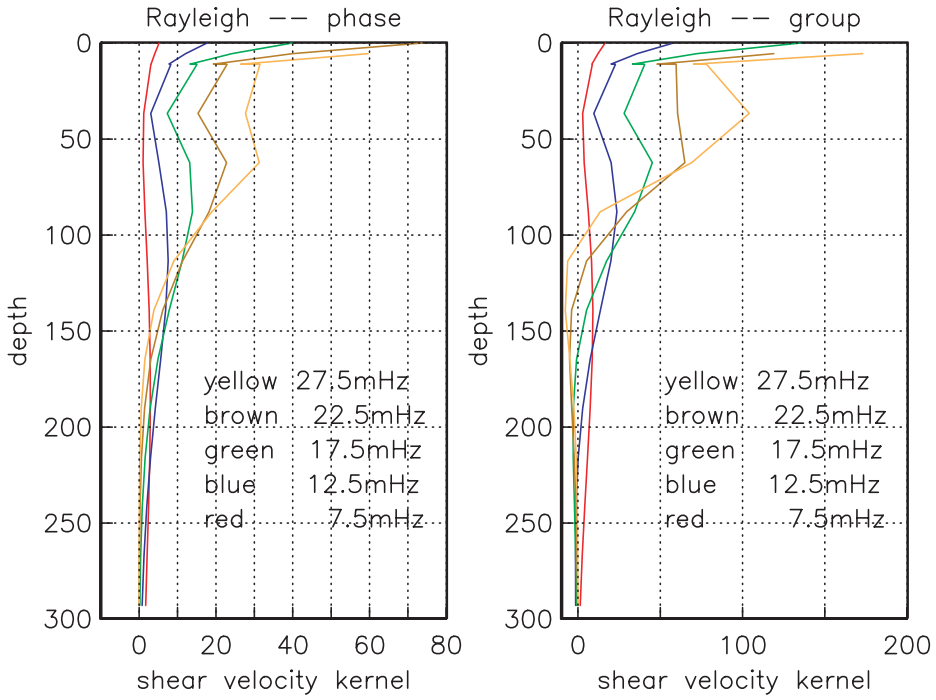

Figure 7 Sensitvity kernels for Rayleigh waves

$$\frac{\delta U}{U} = \frac{\delta c}{c} + \frac{1}{\pi Q_t} \frac{1}{(1+\omega^2\tau^2)}$$

When we use perturbation theory to compute U, we perturb ℓ and compute the corresponding perturbation in frequency, then group velocity is computed by $U = ad\omega/d\ell$ where a is the radius of the Earth. This works in a non-attenuating Earth without physical dispersion. When we have physical dispersion, most codes that compute mode frequencies does the physical dispersion correction to the elastic moduli so that the perturbation to the phase velocity is already accounted for. Thus $\delta c/c$ is effectively zero and the correction to our computed group velocity is just the last term in this equation. Let U_p be the computed group velocity from perturbation theory, then, the actual group velocity is given by

$$U = U_p \left[1 + \frac{1}{\pi Q_t}\right]$$

This equation is valid for the standard dispersion model. The effect of making this correction is shown in the accompanying powerpoint.

6.8 Ray tracing and arrival angles . In this section, we consider the effect of 3D structure on a surface wave "wave front". For ray theory to be valid, we assume that the structural wavelength must be much larger than the wavelength or our signal. If the structural wavelength in the medium and the characteristic wavelength of the signal are of the same order of magnitude, ray theory will bias apparent velocities towards higher values. E.g. in the case of a low velocity anomaly, arrivals of faster waves which were diffracted into the surrounding medium (which are not modelled by ray theory) may be mispicked as arrivals of the wave travelling through the low velocity body.

For surface waves, in contrast to ray theory for body waves, depth-dependent velocity structure is involved only indirectly through a frequency-dependent phase velocity $c(\omega)$. Hence, surface wave ray tracing allows a discontinuous velocity-depth function. In order to have variations in the wave field in each direction of similar length scale, motion is described in a stretched coordinate system with

$$X = \epsilon x, \quad Y = \epsilon y, \quad Z = z, \quad \tau = \epsilon t.$$

The number ϵ is small and indicates the order of lateral heterogeneity. The elastic parameters are then

$$\lambda = \lambda(z, \epsilon x, \epsilon y); \quad \mu = \mu(z, \epsilon x, \epsilon y); \quad \rho = \rho(z, \epsilon x, \epsilon y)$$

The general trial solution for the wave equation looks like

$$\mathbf{u}(x,y,z,t) = e^{i\Psi(x,y,t)} \underbrace{\sum_{n=0}^{\infty} \mathbf{U}_n(X,Y,Z,\tau)\epsilon^n}_{A(\mathbf{x},t)} . \tag{6.13}$$

For $\epsilon = 0$, there are two solutions to the wave equation: one for Love waves and one for Rayleigh waves. In this case (the zeroth approximation), they are decoupled and can be investigated independently. Substitution of (6.13) into the equations of motion finally leads to the eikonal equation:

$$(\nabla T)^2 = n^2 = \frac{1}{c^2}$$

where $c = c(\omega)$ is now the local phase velocity and n is the refractive index (see Aki and Richards, chapter 4 for a discussion of this).

So far, we have not set up a geometric picture of the relationship between the wavefront and the corresponding rays. Suppose a point on a travelling wavefront is given by $t = T(\mathbf{x})$. At time $t + dt$ this point is at $\mathbf{x} + d\mathbf{x}$ and the travel time of the point is

$$t + dt = T(\mathbf{x} + d\mathbf{x}) = T(\mathbf{x}) + \nabla T d\mathbf{x}; \quad \text{with} \quad dt = \nabla T d\mathbf{x}$$

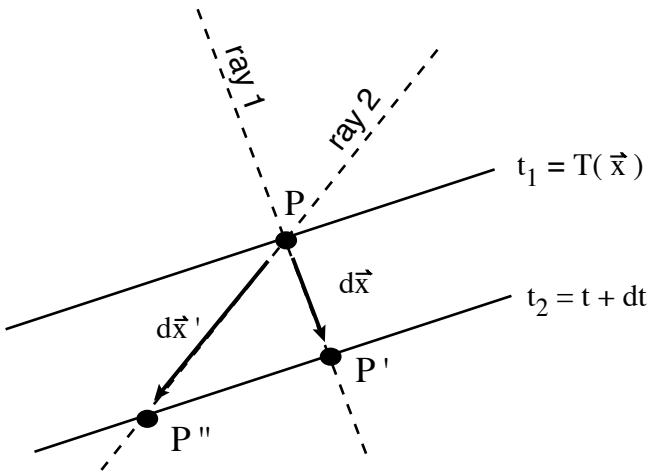

Figure 8

so we get

$$1 = \nabla T \frac{d\mathbf{x}}{dt}$$

where $\mathbf{v} = d\mathbf{x}/dt$ is the travelling speed of the point. $\mathbf{v}$ and $1/\nabla T$ are only equal if they are parallel meaning that the ray is perpendicular to the wavefront (ray 1 in Fig. 6.8). If the ray is not perpendicular to the wavefront (ray 2, e.g. anisotropic media), a point on the wavefront travels a longer distance $d\mathbf{x}'$ for the wavefront moving with the same apparent velocity $1/\nabla T$, so

$$\mathbf{v} \cdot \mathbf{v} \geq \frac{1}{(\nabla T)^2} = c^2.$$

The unit normal of the wavefront is $c\nabla T$. If the rays are practically perpendicular to the wavefront (i.e. derivatives perpendicular to the wavefront are much larger than parallel to it), the travel distance of a point on the wavefront is $d\mathbf{x} = c\nabla T ds$ where ds is the arc length increment. So

$$\frac{d\mathbf{x}}{ds} = c\nabla T.$$

Let $\mathbf{f} = \frac{1}{c}\frac{d\mathbf{x}}{ds}$ and differentiate with respect to s

$$\frac{d\mathbf{f}}{ds} = \frac{d}{ds}\nabla T = \left(\frac{d\mathbf{x}}{ds}\nabla\right)\nabla T = c\nabla T \nabla(\nabla T) = \nabla\left(\frac{1}{c}\right).$$

So the set of *ray tracing equations* become

$$\mathbf{f} = \frac{1}{c}\frac{d\mathbf{x}}{ds}; \qquad \frac{d\mathbf{f}}{ds} = \nabla\left(\frac{1}{c}\right). \tag{6.14}$$

The ray tracing equations may be solved with the *shooting method* using a Runge-Kutta integration. The starting point is fixed and a trial value is chosen for the initial direction, or take-off angle, of the ray. Corrections are made to the take-off angle until the ray passes the end point within a desired distance limit. Another approach is the *bending method* where both the source and the receiver locations are fixed and a trial path between the two station is chosen as initial guess. This path is changed until it satisfies the differential equations.

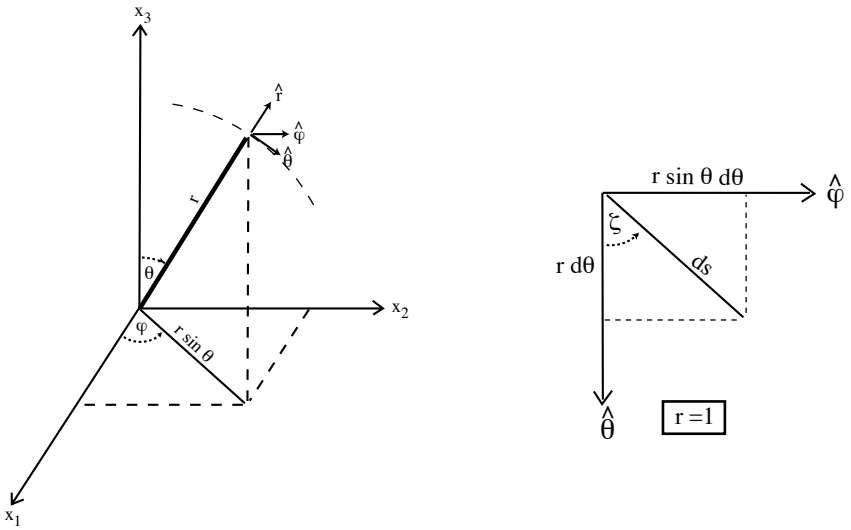

Figure 9

6.9 Surface Wave Ray Tracing on a Sphere .

The only component we have to consider is the f_3–component since on a spherical surface every point is uniquely determined by $z = z(x, y)$. From Fig. 6.9 we get, for a unit sphere,

$$\frac{d\theta}{ds} = \cos\zeta, \qquad \frac{d\phi}{ds} = \frac{\sin\zeta}{\sin\theta}, \quad \text{so} \quad \frac{d\theta}{d\phi} = \cot\zeta\sin\theta \tag{6.15}$$

where ds is the arc length increment on the surface of the unit sphere. The relationship between the components of vector **f** in cartesian and in spherical coordinates is expressed by the transformation matrix

$$\begin{pmatrix} f_1 \\ f_2 \\ f_3 \end{pmatrix} = \begin{pmatrix} \sin\theta\cos\phi & \cos\theta\cos\phi & -\sin\phi \\ \sin\theta\sin\phi & \cos\theta\sin\phi & \cos\phi \\ \cos\theta & -\sin\theta & 0 \end{pmatrix} \begin{pmatrix} f_r \\ f_\theta \\ f_\phi \end{pmatrix} \tag{6.16}$$

and the third component of $\nabla(\frac{1}{c})$ becomes

$$\frac{\partial}{\partial x_3}\left(\frac{1}{c}\right) = \cos\theta\frac{\partial}{\partial r}\left(\frac{1}{c}\right) - \sin\theta\frac{\partial}{\partial\theta}\left(\frac{1}{c}\right). * \tag{6.17}$$

Since r does not change along ds

$$\begin{aligned} \frac{dx_3}{ds} &= \cos\theta\frac{dr}{ds} - \sin\theta\frac{d\theta}{ds} = -\sin\theta\frac{d\theta}{ds} \\ \frac{d}{ds} &= \frac{d\theta}{ds}\frac{\partial}{\partial\theta} + \frac{d\phi}{ds}\frac{\partial}{\partial\phi} = \cos\zeta\frac{\partial}{\partial\theta} + \frac{\sin\zeta}{\sin\theta}\frac{\partial}{\partial\phi}. \end{aligned} \tag{6.18}$$

* remember that in spherical coordinates

$$\nabla\Psi = \hat{r}\frac{\partial\Psi}{\partial r} + \hat{\theta}\frac{1}{r}\frac{\partial\Psi}{\partial\theta} + \hat{\phi}\frac{1}{r\sin\theta}\frac{\partial\Psi}{\partial\phi}$$

and that we have a unit sphere, so $r = 1$.

Then (together with 6.15), the third components of equations (6.14) become

$$cf_3 = -\sin\theta\cos\zeta, \quad \frac{df_3}{ds} = \cos\theta\frac{\partial}{\partial r}\left(\frac{1}{c}\right) - \sin\theta\frac{\partial}{\partial\theta}\left(\frac{1}{c}\right).$$

Differentiating the first equation by s and substituting the second equation into the new equation, and with $\partial\, ln\, c = (1/c)\partial c = -c\partial(1/c)$ we finally get an expression for $d\zeta/ds$. We also use $\partial ln\, c/\partial r = 1$, since this has to be true if the ray is to stay on the surface of the Earth. $d\zeta/ds$ becomes

$$-\frac{\cos\zeta}{\sin\theta}\frac{\partial\, ln\, c}{\partial\phi} + \sin\zeta\frac{\partial\, ln\, c}{\partial\theta} + \cot\theta\sin\zeta = \frac{d\zeta}{ds}. \tag{6.19}$$

For further simplification of the ray tracing equation it is helpful to use a different set of spherical surface coordinates. Some authors use the coordinates of the Mercator projection with $x_1 = \phi, x_2 = ln(\tan(\frac{\theta}{2}))$. In this coordinate system, the ray tracing equations are those of a cartesian coordinate system and ray tracing routines which are written for 2-D body wave ray tracing can be applied to surface waves propagating on a spherical surface without change. We use a slightly different coordinate system with $x_1 = \gamma \equiv \cot\theta$ and $x_2 = \phi$ with θ, ϕ being colatitude and longitude (Fig. 6.10). The advantage of this coordinate system is that the ray tracing equations can be reduced to an almost linear second order differential equation in the case of weak heterogeneity in the medium.

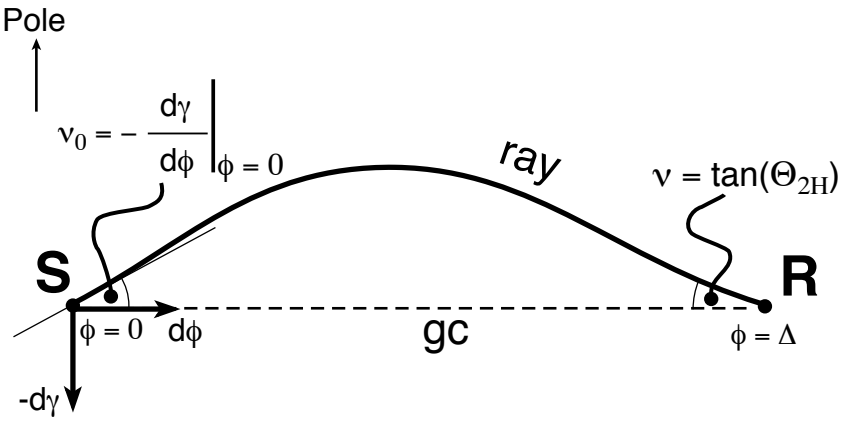

Figure 10 Ray geometry of a true ray for surface waves from the source (S) to the receiver (R) through a heterogeneous medium. It is convenient to rotate the great circle (GC) into the equator. See text for details.

The infinitesimal length increments on the surface of the unit sphere in each coordinate direction are $dx_1 = d\theta$ and $dx_2 = \sin\theta d\phi$. With

$$d\gamma = -\frac{1}{\sin^2(\theta)}d\theta = -(\gamma^2+1)d\theta; \qquad \sin\theta = \frac{1}{\sqrt{\gamma^2+1}}$$

it follows that

$$dx_1 = \frac{-1}{\gamma^2+1}d\gamma; \qquad dx_2 = \frac{1}{\sqrt{\gamma^2+1}}d\phi.$$

With $\nu = -d\gamma/d\phi$ we can write the arc length increment as

$$ds = \sqrt{dx_1^2 + dx_2^2} = d\phi\sqrt{\frac{\nu^2}{(1+\gamma^2)^2} + \frac{1}{1+\gamma^2}}. \tag{6.20}$$

With $\theta = \theta(\phi)$ we also have

$$\nu = -\frac{d\gamma}{d\phi} = -\frac{d\gamma}{d\theta}\frac{d\theta}{d\phi} = \frac{\cot\zeta}{\sin\theta} \tag{6.21}$$

From (6.21) it follows that

$$\frac{d^2\gamma}{d\phi^2} = -\frac{d}{d\phi}\left(\frac{\cot\zeta}{\sin\theta}\right) = \frac{1}{\sin\theta\,\sin^2\zeta}\frac{d\zeta}{d\phi} - \frac{\cot\zeta\cot\theta}{\sin\theta}\frac{d\theta}{d\phi}.$$

with

$$\frac{d\zeta}{d\phi} = \frac{d\zeta}{ds}\frac{ds}{d\phi} \qquad \text{and} \qquad \frac{1}{\sin^2\zeta} = 1 + \frac{\nu^2}{1+\gamma^2},$$

after some trigonometry, we finally get

$$\frac{d^2\gamma}{d\phi^2} + \gamma = \left(1 + \frac{\nu^2}{1+\gamma^2}\right)(\partial_\theta - \nu\partial_\phi)\,ln\,c(\theta,\phi). \tag{6.22}$$

Remember that the phase velocity is $c = \omega/k$ and $\nu \equiv -d\gamma/d\phi$ the tangent of the ray azimuth, measured clockwise from the great circle direction. ∂_θ and ∂_ϕ are the partial derivatives $\partial/\partial\theta$ and $\partial/\partial\phi$.

It is convenient to rotate the source-receiver great circle onto the equator where the coordinates of source and receiver are $\phi_s = 0$, $\phi_r = \Delta$ and $\theta_s, \theta_r = \pi/2$ with Δ being epicentral distance (Fig. 6.10). With this rotation, the ray centered coordinate system is transformed so that the arc length is approximately described by ϕ and the deviation of the ray path from the great circle ($\gamma = 0$) by $\gamma(\phi)$. In this coordinate system, the boundary conditions for (6.22) are simply

$$\gamma(0) = \gamma(\Delta) = 0 \tag{6.23}$$

where (6.22) and (6.23) may be solved numerically with the shooting method and a Runge-Kutta algorithm with an initial guess for the take-off angle $\nu(0) = \nu_0$ and $\gamma(0) = 0$ as starting solution.

6.10 The Path Integral Approximation for the Phase and Fermat's Principle . We now show that the phase integral derived from the theory above is actually the one obtained from Fermat's principle. Hence, even though the polarization angle is not stationary with respect to small changes in structure, the theory (since it is consistent with Fermat's principle for the phase) can be used for a first order approximation.

For a homogeneous Earth, equation (6.22) can be immediately solved, subject to the boundary condition (6.23), and the solutions are:

$$\gamma(\phi) = 0 \qquad \nu(\phi) = 0.$$

In a slightly heterogeneous earth with $\delta c/c$ being small and smooth, the velocity derivatives are also small

$$\partial_\theta\,ln\,c = O(\epsilon),\ \partial_\phi\,ln\,c = O(\epsilon) \tag{6.24}$$

and the solutions can be represented by

$$\gamma(\phi) = O(\epsilon) \qquad \nu(\phi) = O(\epsilon). \tag{6.25}$$

The phase integral along the ray is

$$\Psi = \omega T = \omega \int_{ray} \frac{ds}{c}$$

where c is the local phase velocity. With respect to a spherically symmetric earth model, the perturbation in the phase is expressed by

$$\delta\Psi = \omega \int\limits_{ray} \frac{ds}{c} - \frac{\omega a}{c_0}\Delta. \tag{6.26}$$

With the arc length increment of (6.20) this expression can be written

$$\delta\Psi = \frac{\omega a}{c_0} \int\limits_0^{\Delta} \left[\frac{c_0}{c} \underbrace{\left\{ \frac{\nu^2}{(1+\gamma^2)^2} + \frac{1}{1+\gamma^2} \right\}^{\frac{1}{2}}}_{D} - 1 \right] d\phi. \tag{6.27}$$

For a small heterogeneity the departure of the ray from the equator is small and expression D in the integrand reduces to first order to $D \simeq 1$. Thus, the phase anomaly becomes, to first order,

$$\delta\Psi \simeq \frac{\omega a}{c_0} \int\limits_0^{\Delta} \left[\frac{c_0}{c} - 1 \right] d\phi = -\frac{\omega a}{c_0} \int\limits_0^{\Delta} \frac{\delta c}{c} d\phi$$

and so

$$\delta\Psi \simeq -\frac{\omega a}{c_0} \int\limits_0^{\Delta} \frac{\delta c}{c_0} d\phi \tag{6.28}$$

which is the expression known from Fermat's principle. Thus, the phase integral along the great circle derived from Fermat's principle is correct up to first order changes in the ray trajectory.

6.11 The Path Integral Approximation for the Off-Azimuth Arrival Angle. Unlike the phase, the amplitude and polarization angle of a seismic signal are nonstationary along the ray with respect to small changes in the ray trajectory. However, it is possible to find a linearized approximation analogous to Fermat's Principle. The variation of amplitude (not shown here) and polarization, to first order, can be expressed by a path integral along the source–receiver great circle where variations due to the deformation of the ray path away from the great circle are neglected. In contrast to the phase, the amplitude and polarization depend on the first and second derivatives of the phase velocity in this approximation which enhances resolution for shorter wavelength structure.

For small deviations of the ray path from the great circle, equation (6.22) is almost linear, since ν^2 is very small. A linear differential equation with linear boundary conditions can be solved with a Green's function (Zwillinger, 1992, (Chapter 68., page 268). The Green's function for the left hand side of (6.22) is, subject to boundary condition (6.23):

$$G(\phi, \phi') = \begin{cases} -\operatorname{cosec}\Delta \sin\phi \sin(\Delta - \phi') & \text{for } \phi < \phi' \\ -\operatorname{cosec}\Delta \sin(\Delta - \phi) \sin\phi' & \text{for } \phi > \phi' \end{cases} \tag{6.29}$$

The solution for γ then is

$$\gamma(\phi) = \int\limits_0^{\Delta} G(\phi, \phi') f[\gamma(\phi'), \phi'] d\phi' \tag{6.30}$$

with f being the right hand side of equation (6.22)

$$f = \underbrace{\left(\frac{\nu^2}{1+\gamma^2} + 1 \right)}_{E} \underbrace{\left(\partial_\theta - \nu \partial_\phi \right) ln\, c(\theta, \phi)}_{F}.$$

For small heterogeneity in the velocity, and thus small changes in the ray trajectory the terms E and F are (with (6.24) and (6.25)), to first order:

$$E \simeq 1 \qquad F \simeq \partial_\theta \, ln \, c.$$

Since

$$ln \, c \simeq ln \, c_0 + \frac{1}{c_0}\delta c,$$

integration along the great circle finally leads to

$$\gamma(\phi) \simeq \frac{1}{c_0}\int_0^\Delta G(\phi,\phi')\partial_\theta \delta c(\frac{\pi}{2},\phi')\, d\phi' \tag{6.31}$$

which is the change of the colatitude with longitude along the equator and thus describes the shape of the perturbed ray. Using equation (6.31), the tangent of the take-off angle at the source, $\nu(0)$, and the tangent of the off-azimuth arrival direction at the station, $\nu(\Delta)$, can be easily evaluated as

$$\begin{aligned} \nu(0) = -\frac{d\gamma}{d\phi}_{\phi=0} &= -\int_0^\Delta \frac{d}{d\phi}G(\phi,\phi')\Big|_{\phi=0} f[\gamma(\phi'),\phi']\, d\phi' \\ &\simeq \frac{1}{c_0 \sin\Delta}\int_0^\Delta \sin(\Delta-\phi')\,\partial_\theta \delta c(\frac{\pi}{2},\phi')\, d\phi' \end{aligned} \tag{6.32}$$

and

$$\begin{aligned} \nu(\Delta) = -\frac{d\gamma}{d\phi}_{\phi=\Delta} &= -\int_0^\Delta \frac{d}{d\phi}G(\phi,\phi')\Big|_{\phi=\Delta} f[\gamma(\phi'),\phi']\, d\phi' \\ &\simeq -\frac{1}{c_0 \sin\Delta}\int_0^\Delta \sin\phi'\,\partial_\theta \delta c(\frac{\pi}{2},\phi')\, d\phi'. \end{aligned} \tag{6.33}$$

$\nu(0)$ serves as starting value in the shooting method for exact ray tracing. It is convenient to expand the phase velocity perturbation $\frac{\delta c}{c_0}$ in spherical surface harmonics

$$\frac{\delta c(\theta,\phi)}{c_0} = \sum_l \sum_m c_l^m Y_l^m(\theta,\phi)$$

where l is the harmonic degree and m the azimuthal order with $-l \le m \le l$ and the c_l^m's are complex coefficients and $Y_l^m(\theta,\phi) = X_l^m(\theta)e^{im\phi}$. The tangent of the off-azimuth arrival angle at the station then becomes

$$\nu(\Delta) = -\frac{1}{\sin\Delta}\sum_l \sum_m c_l^m \partial_\theta X_l^m(\frac{\pi}{2})\int_0^\Delta \sin\phi' e^{im\phi'}\, d\phi'. \tag{6.34}$$

Note that in (6.31) the transverse velocity gradient has an increasing weight with a maximum at distance 90° along the ray path. This means that, in the linear approximation, the polarization angle at the station is relatively insensitive to lateral velocity variations in the vicinity of the source but is dominated by local structure if the epicentral distance is less than 90°. The take-off angle, on the other hand, depends strongly upon the velocity structure near the source.

For successive wave trains the off-azimuth arrival angles can be expressed by

$$\nu_n = \begin{cases} -K_1 - \frac{1}{2}(n-1)K_2 & \text{even } n \\ -K_1 + \frac{1}{2}nK_2 & \text{odd } n \end{cases} \tag{6.35}$$

where n is the orbit number of the wave train and K_1 and K_2 the integrals along the source-receiver minor arc and the whole great circle respectively. Equations (6.35) are equations of straight lines with distinct intercepts and opposite slopes, so it is quite obvious that the deviation of the actual ray path from the great circle becomes larger for successive wave trains. For each of the two great circle directions, the K_2-term is accumulated linearly and becomes dominant with increasing wave orbit number. It can be shown that only the X_l^0-terms contribute to the great circle integral. Since $X_l^0(\frac{\pi}{2}) = 0$ for odd l, the integral K_2 depends only on the even order spherical harmonic coefficients of the phase velocity structure and measurements for wave trains with higher orbit number become more and more insensitive to odd order velocity structure.

6.12 Finite frequency kernels . The following is mostly a synopsis of a paper by Zhou et al (2004) (GJI, 158,p142) which discusses the Born approximation to surface wave finite frequency kernels. In the frequency domain, the surface wave seismogram on a spherical Earth can be written as a sum over mode branches:

$$s(\omega) = \sum \mathcal{S} \times \left(\frac{e^{-i(k\Delta - n\pi/2 + \pi/4)}}{\sqrt{8\pi k |\sin \Delta|}} \right) \times \mathcal{R}$$

where $\mathcal{S}$ is the branch source term, $\mathcal{R}$ is the receiver term and the expression in the middle gives the geometrical propagation term. In the presence of 3D structure, the displacement field is perturbed:

$$s(\omega) \to s(\omega) + \delta s(\omega)$$

and, in the Born approximation, $\delta s(\omega)$ is given by

$$\delta s(\omega) = \sum_{\sigma' \sigma''} \int \mathcal{S}' \times \left(\frac{e^{-i(k'\Delta' - n'\pi/2 + \pi/4)}}{\sqrt{8\pi k' |\sin \Delta'|}} \right) \times {}_{\sigma'}\Omega_{\sigma''} \times \left(\frac{e^{-i(k''\Delta'' - n''\pi/2 + \pi/4)}}{\sqrt{8\pi k'' |\sin \Delta''|}} \right) \times \mathcal{R}''\, dV$$

This equation represents the history of wave propagation. We go from source excitation to propagation to the scatterer, there is a possibility of mode conversion (the Ω term), then we propagate to the receiver. Suppose we have estimated the transfer function between $s(\omega)$ (the synthetic) and $s(\omega) + \delta s(\omega)$ (the observed seismogram):

$$s(\omega) + \delta s(\omega) = T(\omega) s(\omega)$$

and we let $T = 1 + \delta T$. Writing $s = A \exp(i\Psi)$ and $s + \delta s = (A + \delta A) \exp(i(\Psi + \delta\Psi)$ shows the phase of the transfer function is given by

$$\delta\Psi(\omega) = \text{Im}\left(\frac{\delta s}{s}\right)$$

and

$$\frac{\delta A}{A} = \text{Re}\left(\frac{\delta s}{s}\right)$$

Substituting in the above expressions for s and δs gives

$$\delta\Psi(\omega) = \int_V K_\Psi \delta m\, dV$$

where

$$K_\Psi = -\text{Im}\left(\sum_{\sigma'\sigma''} \frac{\mathcal{S}'_{\sigma'}\Omega_{\sigma''}\mathcal{R}'' e^{-i(k'\Delta'+k''\Delta''-k\Delta-(n'+n''-n)\pi/2+\pi/4)}}{\mathcal{S}\mathcal{R}\sqrt{8\pi k'k''/k\,(|\sin\Delta'||\sin\Delta''|/|\sin\Delta|)}}\right)$$

Under some assumptions, this 3D kernel can be reduced to a 2D kernel. In particular, we have to ignore mode coupling effects which is probably reasonable for fundamental modes and assume forward scattering. In that case, the depth integral becomes ($\sigma' = \sigma'' = \sigma$):

$$\int_0^a {}_{\sigma'}\Omega_{\sigma''} \frac{\delta m}{m} r^2\, dr = -2k^2 \frac{\delta c}{c}$$

and we have

$$\delta\Psi(\omega) = \int_\Omega K_\Psi \frac{\delta c}{c}\, d\Omega$$

where

$$K_\Psi = \text{Im}\left(\frac{2k^2\mathcal{S}'\mathcal{R}'' e^{-i[k(\Delta'+\Delta''-\Delta)-(n'+n''-n)\pi/2+\pi/4]}}{\mathcal{S}\mathcal{R}\sqrt{8\pi k\,(|\sin\Delta'||\sin\Delta''|/|\sin\Delta|)}}\right)$$

Further simplification can be had by ignoring the effect of source radiation ($\mathcal{S} \simeq \mathcal{S}'$) and by ignoring the difference in direction between the direct and scattered radiation at the receiver ($\mathcal{R} \simeq \mathcal{R}'$). For the minor arc ($n' + n'' = n = 1$) then

$$K_\Psi = \text{Im}\left(\frac{2k^2 e^{-i[k(\Delta'+\Delta''-\Delta)+\pi/4]}}{\sqrt{8\pi k\,(|\sin\Delta'||\sin\Delta''|/|\sin\Delta|)}}\right)$$

This kernel can be easily calculated as it involves only geometrical terms. Clearly, the critical term is the difference in path length $\Delta' + \Delta'' - \Delta$ which is the difference in path travelled to and from the scatterer minus the distance travelled by the direct wave. If this distance is small, the scattered energy will interfere constructively with the direct energy and we will get a region of positive sensitivity around the direct ray. As we go further away from the ray path, we may end up interfering destructively with the direct energy. Thus the 2D kernel has side lobes – both positive and negative, corresponding roughly to Fresnel zones. The kernel described above is for a single frequency but real measurements include a range of frequencies and this tends to suppress side lobes in the 2D kernel because the side lobes associated with different frequencies tend to cancel each other out. Examples will be given in the accompanying powerpoint.

Finally, note that the kernel for amplitude perturbations ($\delta A/A$ is just given by the real part of the above kernel (see below).

6.13 Anisotropy . These notes are from the paper by Smith and Dahlen (1973). Consider a cartesian coordinate system with x pointing north, y pointing east and z pointing down. $\mathbf{k}$ is the horizontal wave number ($\hat{\mathbf{z}} \cdot \mathbf{k} = 0$). The dispersion relation is $\omega(\mathbf{k})$ and the phase velocity is $c(\mathbf{k})$ defined by

$$c(\mathbf{k}) = \frac{\omega(\mathbf{k})}{k} \quad \text{where} \quad k = \sqrt{\mathbf{k}\cdot\mathbf{k}}$$

It is convenient to think of the phase velocity not as a function of $\mathbf{k}$ but as a function of ω and of the wave vector direction: $\hat{\mathbf{k}} = \mathbf{k}/k$. Consider a single station at a direction $\hat{\mathbf{n}}$ pointing from source to receiver. A phase measurement will yield an apparent phase velocity $c(\omega, \hat{\mathbf{n}})$ of waves whose group velocity has direction $\hat{\mathbf{n}}$. Let the group velocity with wave number $\mathbf{k}$ be $\mathbf{U}(\mathbf{k}) = U(\mathbf{k})\hat{\mathbf{n}}(\mathbf{k})$ where

$$\mathbf{U}(\mathbf{k}) = \nabla_{\mathbf{k}}\,\omega(\mathbf{k}) \quad \text{and} \quad U(\mathbf{k}) = \sqrt{\mathbf{U}(\mathbf{k})\cdot\mathbf{U}(\mathbf{k})}$$

Phase velocity measurements in general provide the quantity

$$C(\omega(\mathbf{k}), \hat{\mathbf{n}}(\mathbf{k})) = \left[\frac{\hat{\mathbf{n}}(\mathbf{k}) \cdot \mathbf{k}}{\omega(\mathbf{k})}\right]^{-1}$$

We are interested in a medium that has only slight anisotropy. In such a medium, the group direction $\hat{\mathbf{n}}(\mathbf{k})$ can differ from $\mathbf{k}$ only by a first-order rotation about the $\hat{\mathbf{z}}$ axis:

$$\hat{\mathbf{n}}(\mathbf{k}) = \hat{\mathbf{k}} + \hat{\boldsymbol{\theta}} f(\mathbf{k}) \quad \text{where} \quad \hat{\boldsymbol{\theta}} \cdot \hat{\mathbf{k}} = 0 \quad \text{and} \quad \hat{\boldsymbol{\theta}} \cdot \hat{\mathbf{z}} = 0$$

and where $f(\mathbf{k})$ is a term of first order in anisotropy. This has two consequences. The first is that $C(\omega(\mathbf{k}), \hat{\mathbf{n}}(\mathbf{k})) = C(\omega(\mathbf{k}), \hat{\mathbf{k}})$ to first order – this means that the apparent phase velocity measured in the $\hat{\mathbf{n}}$ direction is the same as the apparent phase velocity in the $\hat{\mathbf{k}}$ direction. The second consequence is that $C(\omega(\mathbf{k}), \hat{\mathbf{n}}(\mathbf{k})) = c(\omega(\mathbf{k}), \hat{\mathbf{k}})$ to first order – the measured phase velocity in the direction $\hat{\mathbf{n}}$ is equal to the true phase velocity in the direction $\hat{\mathbf{k}}$. Thus

$$C(\omega(\mathbf{k}), \hat{\mathbf{k}}) = c(\omega(\mathbf{k}), \hat{\mathbf{k}})$$

Phase velocity measurements as a function of azimuth θ therefore provide a direct determination of $c(\omega, \theta)$ where θ is the azimuth of $\hat{\mathbf{k}}$. Smith and Dahlen also show that (correct to first order)

$$\Gamma(\omega(\mathbf{k}), \hat{\mathbf{k}}) = c(\omega(\mathbf{k}), \hat{\mathbf{k}}) + k\partial_k c(\omega(\mathbf{k}), \hat{\mathbf{k}})$$

where Γ is the measured group velocity of waves whose wave group points in the direction $\hat{\mathbf{k}}$. We now consider a weakly anisotropic half space specified by its density $(\rho(z))$ and its elastic tensor $E_{ijkl}(z)$. Let $\mathbf{u}(\mathbf{r}, t)$ be the elastic displacement field and let $\omega(\mathbf{k})$ be the frequency of surface wave propagation along the surface, then

$$\mathbf{u}(\mathbf{r}, t) = \mathbf{s}(z) \exp i[\mathbf{k} \cdot \mathbf{r} - \omega(\mathbf{k})t]$$

where $\mathbf{s}(z)$ is complex and suitably decaying at large depth. The strain tensor is given by

$$\boldsymbol{\epsilon}(\mathbf{r}, t) = \tfrac{1}{2}\left[\nabla \mathbf{u} + (\nabla \mathbf{u})^T\right]$$

and the associated stress tensor is

$$\mathbf{T}(\mathbf{r}, t) = \mathbf{E} : \boldsymbol{\epsilon}$$

Equating the kinetic and elastic potential energies (remember we are neglecting all gravitational effects) then

$$\omega^2 \int_0^\infty \rho \mathbf{u} \cdot \mathbf{u}^* dz = \int_0^\infty \mathbf{T} : \boldsymbol{\epsilon}^* dz$$

where the asterisk denotes complex conjugation. Rayleigh's principle guarantees that ω^2 is stationary with respect to small perturbations in $\mathbf{s}(z)$ (provided that $\mathbf{s}(z)$ is a valid surface wave displacement field). Thus Rayleigh's principle can be used to compute to first order the effect of a small perturbation in properties on $\omega^2(\mathbf{k})$ (see chapter 4). Let us suppose that $\mathbf{E}(z) = \mathbf{E}_0(z) + \boldsymbol{\gamma}(z)$ where $\boldsymbol{\gamma}$ is small relative to $\mathbf{E}_0$. Then we have

$$\delta\omega^2(\mathbf{k}) = \frac{\int_0^\infty \gamma_{ijkl} \epsilon_{ij} \epsilon_{jk}^* dz}{\int_0^\infty \rho u_i u_i^* dz}$$

Then, from $c(\mathbf{k}) = \omega(\mathbf{k})/k$, we have

$$\delta c(\mathbf{k}) = \frac{c}{2\omega^2} \frac{\int_0^\infty \gamma_{ijkl}\epsilon_{ij}\epsilon^*_{jk}dz}{\int_0^\infty \rho u_i u_i^* dz}$$

Note that this is the perturbation in the phase velocity at fixed wave number though we usually make the measurements at fixed frequency and $\delta c(\omega) = c/U\delta c(k)$. We now assume the underlying medium is isotropic (more generally, transversely isotropic) so the form for E_0 is well-known. Any fourth order elastic tensor satisfying the usual symmetries has 21 independent coefficients. Backus (1970) shows that these 21 coefficients can be expressed as a linear combination of 21 canonical harmonic tensors of degrees 0,2, and 4. Smith and Dahlen use Backus' results though a more direct approach is used by Montagner and Nataf 1986). In any case, for Love waves, we find:

$$\delta c_L(\mathbf{k},\theta) = \frac{1}{2c_L}\left[L_1(\omega) + L_2(\omega)\cos(2\theta) + L_3(\omega)\sin(2\theta) + L_4\cos(4\theta) + L_5(\omega)\sin(4\theta)\right]$$

where the L's are integrals over depth of combinations of the elastic coefficients weighted with the eigenfunction. Defining $L_0 = \int \rho W^2 dz$, we find

$$\begin{aligned}
L_1 &= \frac{1}{L_0}\int (W^2 dN + \frac{W'^2}{k^2}dL)dz \\
L_2 &= \frac{1}{L_0}\int -G_c\frac{W'^2}{k^2}dz \\
L_3 &= \frac{1}{L_0}\int -G_s\frac{W'^2}{k^2}dz \\
L_4 &= \frac{1}{L_0}\int -C_c W^2 dz \\
L_5 &= \frac{1}{L_0}\int -C_s W^2 dz
\end{aligned}$$

There is a similar relationship for Rayleigh waves but with the L's replaced by the following R's. Defining $R_0 = \int \rho(U^2+V^2)dz$, we find

$$\begin{aligned}
R_1 &= \frac{1}{R_0}\int [V^2 dA + \frac{U'^2}{k^2}dC + \frac{2U'V}{k}dF + (\frac{V'}{k} - U)^2 dL]dz \\
R_2 &= \frac{1}{R_0}\int [B_c V^2 + H_c\frac{2U'V}{k} + G_c(\frac{V'}{k} - U)^2]dz \\
R_3 &= \frac{1}{R_0}\int [B_s V^2 + H_s\frac{2U'V}{k} + G_s(\frac{V'}{k} - U)^2]dz \\
R_4 &= \frac{1}{R_0}\int C_c V^2 dz \\
R_5 &= \frac{1}{R_0}\int C_s V^2 dz
\end{aligned}$$

Note that L_1 and R_1 are sensitive only to A, C, N, L and F which are the elastic constants defining a transversely isotropic material. In terms of γ_{ij} (Voigt notation)

$$
\begin{aligned}
dA &= \frac{3}{8}(\gamma_{11} + \gamma_{22}) + \frac{1}{4}\gamma_{12} + \frac{1}{2}\gamma_{66} \\
dC &= \gamma_{33} \\
dF &= \frac{1}{2}(\gamma_{13} + \gamma_{23}) \\
dL &= \frac{1}{2}(\gamma_{44} + \gamma_{55}) \\
dN &= \frac{1}{8}(\gamma_{11} + \gamma_{22}) - \frac{1}{4}\gamma_{12} + \frac{1}{2}\gamma_{66}
\end{aligned}
$$

The 2θ terms are

$$
\begin{aligned}
B_c &= \frac{1}{2}(\gamma_{11} - \gamma_{22}) \\
G_c &= \frac{1}{2}(\gamma_{55} - \gamma_{44}) \\
H_c &= \frac{1}{2}(\gamma_{13} - \gamma_{23}) \\
B_s &= \gamma_{16} + \gamma_{26} \\
G_s &= \gamma_{54} \\
H_s &= \gamma_{36}
\end{aligned}
$$

The 4θ terms are

$$
\begin{aligned}
C_c &= \frac{1}{8}(\gamma_{11} + \gamma_{22}) - \frac{1}{4}\gamma_{12} - \frac{1}{2}\gamma_{66} \\
C_s &= \frac{1}{2}(\gamma_{16} - \gamma_{26})
\end{aligned}
$$

Montagner and Nataf (1986) show that for a reasonable form of the anisotropy (e.g. alignment of olivine crystals), the 2θ terms dominate for Rayleigh waves and, in our inversions, we have found the 4θ terms to be insignificant. For Love waves, the 4θ terms can be as large or larger than the 2θ terms but they require very good azimuthal coverage to recover. In our Love wave inversions, we have not found azimuthal anisotropy to help significantly improve the fit to the data.

Ekstrom (2011) has shown that the 2θ terms for Rayleigh waves must be included as there are tradeoffs with the R_1 terms. These tradeoffs lead to artifacts in the form of streaks in the Pacific Ocean. Azimuthal anisotropy is fairly weak and long paths over coherent anisotropy are required to accumulate a detectable signal. For this reason, azimuthal anisotropy is well–determined only in oceanic regions. We have also found that the patterns of fast directions of anisotropy can tradeoff with event locations (see accompanying powerpoint for some results).

6.14 Amplitudes and attenuation . The measurement techniques we use to measure phase and group velocity also measure the relative amplitudes of surface wave packets. The fundamental problem is that surface wave amplitudes are impacted by many things and intrinsic attenuation is a relatively minor contributor. In this work, we follow the basic procedure described by Dalton and Ekstrom (2006) where the observed surface wave amplitude anomaly is expressed as

$$
A(\omega) = A_S(\omega)A_I(\omega)A_F(\omega)A_Q(\omega) \tag{36}
$$

where A_S and A_I are due to uncertainties in earthquake size and instrument responses, A_F is due to focusing-defocusing effects and A_Q is due to attenuation structure. Note that this expression neglects some possibly important effects, such as overtone interference, but we shall adopt it initially. The first two effects are relatively easy to deal with, but the method of dealing with A_F can be important. Dalton and Ekstrom (2006) use the ray-theoretical formulation of Woodhouse and Wong (1986) to model this effect. As we discuss

below, ray theory gives undue weight to short wavelength structure and its successful use requires careful filtering of the model. We show below that finite frequency kernels (Zhou et al, 2004) seem able to give a more objective treatment of the focusing effects. In a very elegant paper, Woodhouse and Wong (1986) derived an expression for this effect based on ray theory (though see also Dahlen and Tromp, 1998) :

$$\ln A_F = 1/2\text{cosec}\Delta \int_0^{\Delta} \sin(\Delta - \phi)[\sin\phi\partial_\theta^2 - \cos\phi\partial_\phi]\frac{\delta c}{c_0}\, d\phi \tag{37}$$

where Δ is the epicentral distance, ϕ is the along-path coordinate, θ is the path-perpendicular coordinate, and δc is the perturbation in phase velocity. The dominant term in this expression is the second derivative ∂_θ^2 of the phase velocity perturbation. Note that, if the phase velocity perturbation is expanded in spherical harmonics, the second derivative term is of the order of l^2, where l is the spherical harmonic degree. This implies that the focusing-defocusing term predicted by ray theory is highly sensitive to the short-wavelength structure of a phase velocity map. Such structure is often poorly constrained and can be strongly dependent on the nature of damping used in the construction of the map.

Finite frequency effects will mitigate the effect of short wavelength structure and here we consider the 2D approximation to the finite frequency kernel derived by Zhou et al, 2004 (see section on finite frequency kernels):

$$\ln A_F = \int K_A^c \frac{\delta c}{c_0} d\Omega = -\int \frac{2k^2 \cos[k(\Delta' + \Delta'' - \Delta) + \pi/4]}{\sqrt{8\pi k|\sin\Delta'||\sin\Delta''|/|\sin\Delta|}} \frac{\delta c}{c_0} d\Omega \tag{38}$$

where k is the wavenumber, Δ' is the distance between source and scatter, and Δ'' is the distance between scatter and station. Here, we parameterize the phase velocity map in terms of equal area pixels and average the kernel within each pixel of the model. Some care also has to be taken to handle the singularities at the source and receiver. Finally, we employ some frequency averaging to mimic the finite frequency band of the actual measurements. Spetzler et al, 2002 give some analytic results for the frequency integral which can be adapted to the current situation. The frequency averaging attenuates the side-lobes of the kernel and an example of a kernel incorporating these effects is shown in Figure 11 below

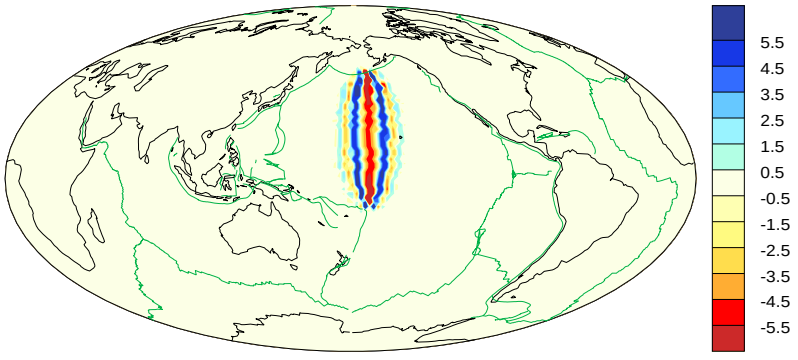

Figure 11 Finite frequency focusing kernel, calculated at 10mHz for an event in Aleutians (01/08/1990) and recorded at station AFI in Samoa. This example parameterizes the phase velocity in 2 degree equal-area pixels

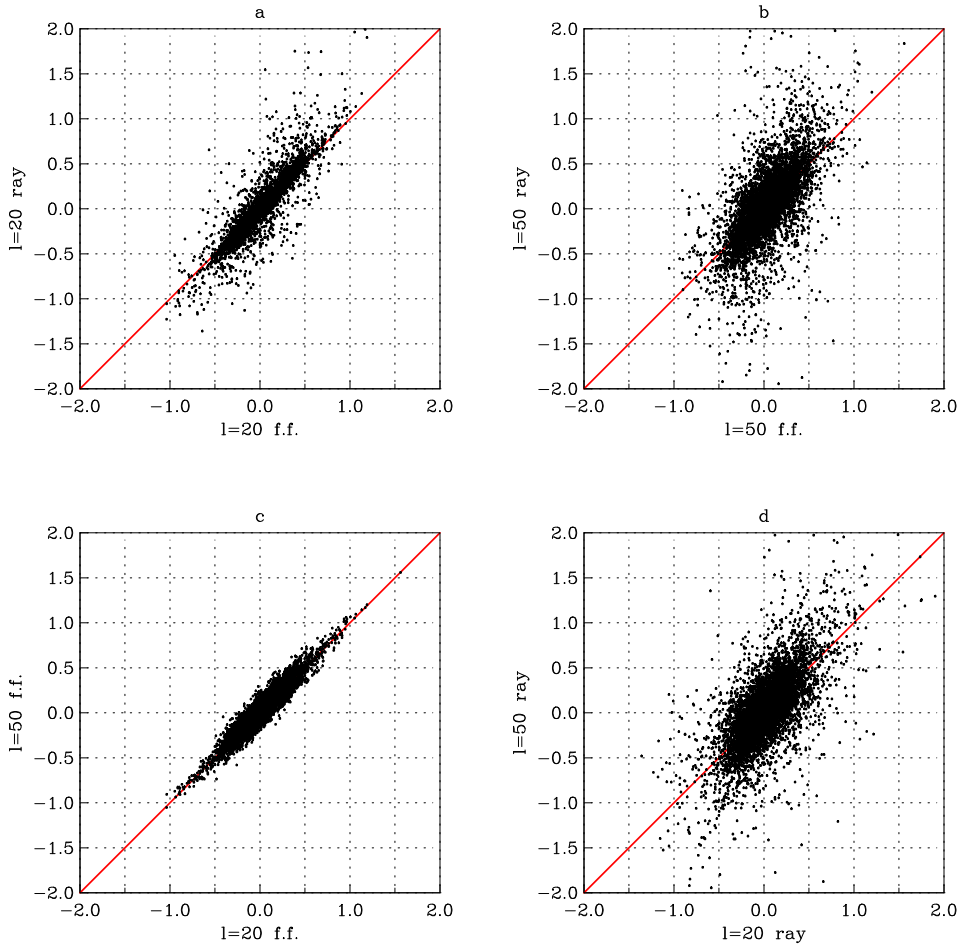

Figure 12 Comparison of focusing-defocusing effect calculated by finite frequency theory (f.f.) and ray theory (ray), from the same map cut off at spherical degree $l = 20$ and $l = 50$. In all cases, $\ln A$ is plotted.

We compare the predictions of ray theory and finite frequency focusing-defocusing effects by doing forward calculations using an existing Rayleigh wave phase velocity map at 100s (Ekstrom, 2011). To evaluate the effect of higher order structure, we perform a spherical harmonic analysis of the map and truncate at different spherical harmonic degrees l. Figure 12c shows that finite frequency theory gives stable result regardless the cut off value of l. The two theories give similar results for a smooth map (Figure 12a), but fail to agree with each other for a rough map (Figure 12b). Ray theory predictions from $l = 20$ and $l = 50$ maps are quite different from each other, which indicates the strong dependence on high order structure (Figure 12d). We conclude from this that ray theory can give useful results if careful attention is paid to how the phase velocity model is smoothed, however, the predictions of the finite frequency kernels appear to be quite robust and suggest that they are better suited as a basis for inversion.

Both the phase delay kernels and the amplitude anomaly kernels in our inversion are calculated based on 2D finite frequency theory (Zhou et al, 2004, Dahlen and Zhou, 2006) and we also include the effects of physical dispersion (Zhou, 2009). Note that Ruan and Zhou (2010) find that 15 to 20% of observed phase anomalies can come from anelastic effects so a joint inversion is needed. We invert for phase velocity perturbations, attenuation perturbations, source terms and receiver terms all at the same time (see equation x):

$$\begin{pmatrix} K_t^c & \frac{c}{2UQ}\left[\frac{2}{\pi}\ln(\frac{\omega}{\omega_0})K_t^c - \frac{K_A^c}{\omega}\right] & 0 & 0 \\ K_A^c & \frac{c}{2UQ}\left[\omega K_t^c + \frac{2}{\pi}\ln(\frac{\omega}{\omega_0})K_A^c\right] & 1 & 1 \\ \lambda_1 D & 0 & 0 & 0 \\ 0 & \lambda_2 D & 0 & 0 \end{pmatrix} \begin{pmatrix} \delta c/c \\ \delta Q^{-1}/Q^{-1} \\ \ln A_s \\ \ln A_r \end{pmatrix} = \begin{pmatrix} \delta t \\ \delta \ln A \\ 0 \\ 0 \end{pmatrix} \tag{39}$$

where the travel time anomaly kernel K_t^c is related to the phase delay kernel in Zhou et al (2004) by

$K^c_\phi = \omega K^c_t$. Physical dispersion uses the standard form when we are in the middle of an absorption band where Q is independent of frequency. The reference frequency ω_0 is typically taken to be 2πrad/s. U is group velocity and D is a roughening operator (a discrete approximation to the 2D Laplacian). λ_1 and λ_2 are smoothing parameters which control the smoothness of the phase velocity and attenuation maps respectively. Note that we are still experimenting with smoothing and that the attenuation maps we present are smoothed much more than the phase velocity maps (which require very little smoothing). The amplitudes of the attenuation maps also tend to be large and imply that different kinds of smoothing may be appropriate.

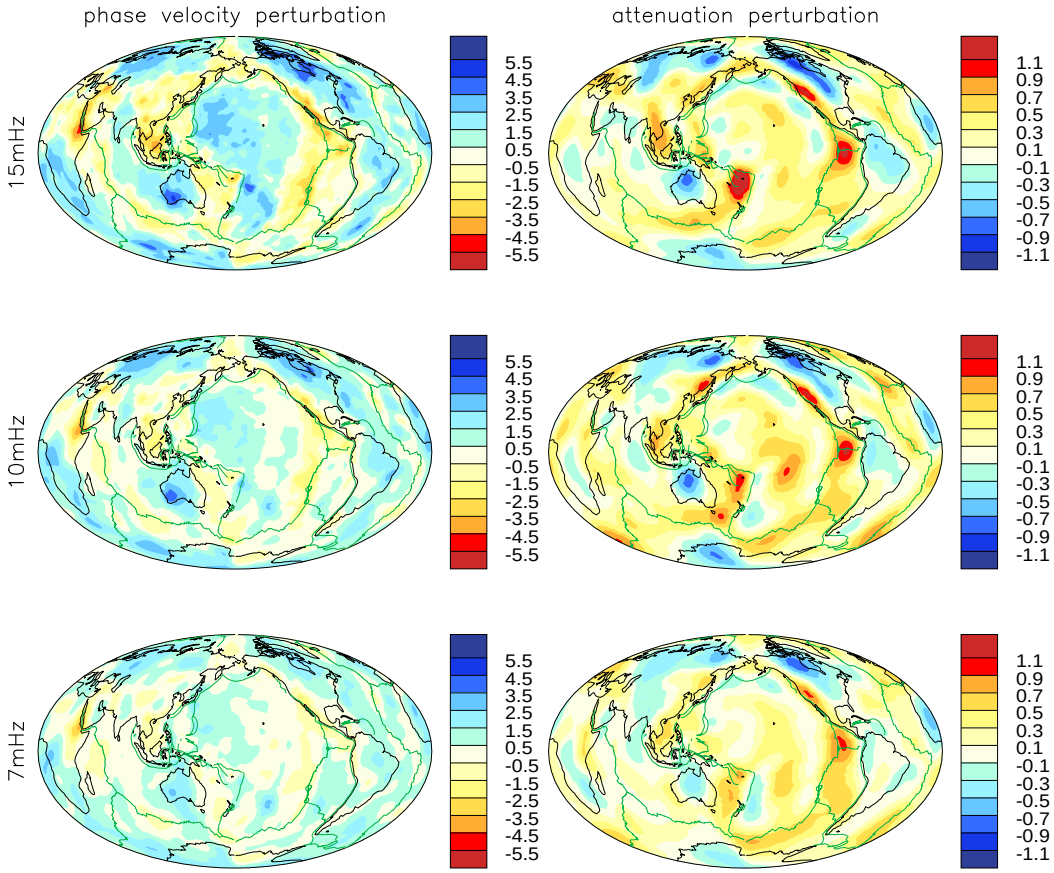

Figure 13. Phase velocity perturbation and attenuation maps for 7mHz, 10mHz and 15mHz. Note that the phase velocity perturbation is in $\delta c/c(\%)$ and attenuation is in $\delta Q^{-1}/Q^{-1}$.

Preliminary results for 7, 10 and 15mHz are shown in Figure 13 As in Dalton and Ekstrom (2006), we obtain high attenuation structures along western America and the East Pacific rise, which indicates that the effect of focusing and defocusing is correctly accounted for (these authors show that these regions can appear to be high Q if the focusing terms are not handled correctly).

In order to understand the relative contributions of the four terms to the amplitude data, we plot the distribution of raw data and the residuals after accounting for different terms (Figure 14). The overall variance reduction reaches 62.2%. However, the attenuation term alone does not improve the fit to the data at all (Figure 14b). It demonstrates again the importance of including the source terms, receiver terms and focusing terms in order to obtain a reasonable attenuation structure. It is in fact the source term that provides the biggest contribution to the variance reduction, in agreement with the results of Dalton and Ekstrom (2006).

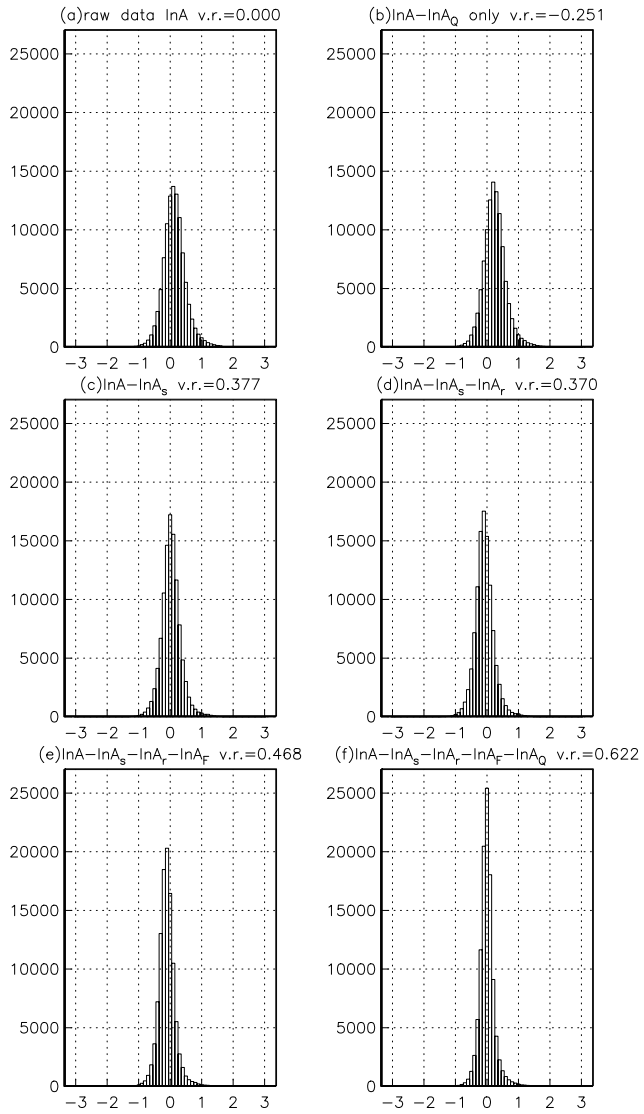

Figure 14. Distribution of raw amplitude data and residuals for 10mHz. (a) Raw data. (b) Residuals after accounting for attenuation terms only – note the negative variance reduction. (c) Residuals after accounting for source terms. (d) Residuals after accounting for source and receiver terms. (e) Residuals after accounting for source, receiver and focusing terms. (f) Residuals after accounting for all four terms. v.r. = variance reduction

6.15 Surface wave waveform modelling . We close this chapter with a description of a method introduced by Woodhouse and Dziewonski (1984) (JGR, 84, 5953) to model waveforms – they used it to model complete waveforms including body waves, but the technique is most appropriate for modelling surface waves. They suggested an ingenious way of incorporating the phase shifts of classical dispersion analysis into the modal representation of the seismogram. The sensitivity of the observables to even order structure then manifests itself as an apparent frequency shift, while the dependence on odd order structure manifests itself as an apparent epicentral distance shift. Suppose we have a "local frequency function" or splitting function

$$\delta\omega(\theta,\phi) = \sum_{s,t} c_s^t Y_s^t(\theta,\phi)$$

where c_s^t are our "structure coefficients" and the sum over s includes odd order structure. The perturbation to the phase of a surface wave can be written

$$\delta\psi = \int_0^T \delta\omega(\theta,\phi)\,dt \tag{6.40}$$

where the integral is with respect to group travel time, i.e.

$$\delta\psi = \frac{T}{x}\int_0^x \delta\omega(\theta,\phi)\,dx' = \frac{1}{U}\int_0^x \delta\omega(\theta,\phi)\,dx' = \int_0^T \delta\omega(\theta,\phi)\,dt.$$

For odd orbits (R_{2n+1}, G_{2n+1})

$$\delta\psi = \int_0^{t_1} \delta\omega(\theta,\phi)\,dt + n\int_0^{T_c} \delta\omega(\theta,\phi)\,dt \tag{6.41}$$

where t_1 is the minor arc group travel time and T_c is the great circle group travel time. For even orbits (R_{2n+2}, G_{2n+2})

$$\delta\psi = \int_0^{\bar{t}_1} \delta\omega(\theta,\phi)\,dt + n\int_0^{T_c} \delta\omega(\theta,\phi)\,dt \tag{6.42}$$

where $\bar{t}_1 = T_c - t_1$. Now let

$$\delta\hat{\omega} = \frac{1}{T_c}\int_0^{T_c} \delta\omega(\theta,\phi)\,dt, \qquad \delta\tilde{\omega} = \frac{1}{t_1}\int_0^{t_1} \delta\omega(\theta,\phi)\,dt \qquad \text{and} \qquad \delta\Delta = \frac{t_1}{l+\frac{1}{2}}\,(\delta\hat{\omega} - \delta\tilde{\omega}) \tag{6.43}$$

then,

$$\begin{aligned}\delta\psi &= nT_c\delta\hat{\omega} + t_1\delta\tilde{\omega} \qquad \text{(odd)}\\ \delta\psi &= nT_c\delta\hat{\omega} + T_c\delta\hat{\omega} - t_1\delta\tilde{\omega} \quad \text{(even)}\end{aligned}$$

or

$$\begin{aligned}\delta\psi &= (nT_c + t_1)\delta\hat{\omega} - t_1(\delta\hat{\omega} - \delta\tilde{\omega}) \qquad \text{(odd)}\\ \delta\psi &= (nT_c + \bar{t}_1)\delta\hat{\omega} + t_1(\delta\hat{\omega} - \delta\tilde{\omega}) \qquad \text{(even)}\end{aligned}$$

and $t_1(\delta\hat{\omega} - \delta\tilde{\omega}) = (l+\frac{1}{2})\delta\Delta$. Our spherical Earth model expansion is (summing over all modes)

$$s = \text{Re}\{\sum_j A_j(\Delta)e^{i\bar{\omega}_j t}\}$$

and becomes

$$s = \text{Re}\{\sum_j A_j(\Delta+\delta\Delta)e^{i(\bar{\omega}_j+\delta\bar{\omega})t}\}. \tag{6.44}$$

Remember that $A_j(\Delta)$ is proportional to $e^{i(l+\frac{1}{2})\Delta}$ in the asymptotic limit of large l. We can therefore include the effects of 3D-structure by a great circle frequency shift (as before) and a shift in epicentral distance which incorporates the effect of odd-order structure. Woodhouse and Dziewonski chose to implement an inversion for 3D-structure using equation (6.40) above by computing differential seismograms relative to a parameterized model. Thus

$$c_s^t = \int_0^a K_s(r)\delta m_s^t(r) r^2\,dr$$

where

$$\delta m(r,\theta,\phi) = \sum \delta m_s^t(r) Y_s^t(\theta,\phi).$$

$\delta m_s^t(r)$ is expanded in a basis set (Woodhouse and Dziewonski chose Legendre functions) so that

$$
\begin{aligned}
\delta m(r,\theta,\phi) &= \sum_{s,t}\sum_{k} {}_k\delta m_s^t f_k(r) Y_s^t(\theta,\phi) \\
c_s^t &= \sum_{k} {}_k\delta m_s^t \underbrace{\int_0^a K_s(r) f_k(r) r^2\, dr}_{D_{sk}}
\end{aligned}
$$

$$
\begin{aligned}
\delta\hat{\omega} =& \frac{1}{T_c}\int_0^{T_c} \sum c_s^t Y_s^t(\theta,\phi)\, dt \\
=& \sum P_s(0) \sum c_s^t Y_s^t(\Theta,\Phi) \\
=& \sum_s P_s(0) \sum_{t,k} {}_k\delta m_s^t D_{sk} Y_s^t(\Theta,\Phi)
\end{aligned}
\tag{6.45}
$$

and

$$
\delta\Delta = \frac{t_1}{l+\frac{1}{2}} \left[\delta\hat{\omega} - \underbrace{\frac{1}{\Delta u}\int_0^{\Delta} \delta\omega(\theta,\phi)\, dx}_{d\tilde{\omega}} \right] \tag{6.46}
$$

Both $\delta\Delta$ and $\delta\hat{\omega}$ can be cast in terms of ${}_k\delta m_s^t$ and derivative seismograms calculated by differentiation of s with respect to ${}_k\delta m_s^t$. An iterative inversion is then based on

$$
{}^s\text{observed} = s_0 + \sum_{k,s,t} \frac{\partial s_0}{\partial\, {}_k\delta m_s^t} \delta({}_k\delta m_s^t). \tag{6.47}
$$

Woodhouse speculated that the source shift that they introduced to model odd order structure was a consequence of along-branch coupling. This was later shown to be the case by Mochizuki (1986), Romanowicz (1987) and Park (1987). The theory admits no coupling between mode branches and so is not good for modelling body waves, however, it is very good for surface-wave equivalent modes and even allows modelling of some low overtone branches. Note that the degree of approximation is the same as some studies which regard the seismogram as a sum of uncoupled mode branches, but has less difficulties in its implementation.